On the transport mechanism of rockfalls and avalanches
by Jeffrey Michael Lacy

A thesis submitted in partial fulfillment of the requirements for the degree OF Master of Science in Engineering Mechanics
Montana State University

Abstract:
In this thesis, a numerical model of a granular shear flow is developed. This model is two-dimensional and assumes the shearing granules to be identical, smooth, semi-elastic circular disks. The field containing these disks is bounded on the top and bottom by solid blocks of disks with the same properties. The field is bounded on the right and left by periodic boundaries. The top boundary block has an assigned horizontal velocity and overburden mass, and is unconstrained in the vertical direction. The base boundary block is immobile and does not permit scour.

The numerical model is then used to test the hypothesis that, for large overburden pressures, collisions in the shearing region occur involving more than two particles, and that these multi-particle collisions act to reduce the shear strength of the dilatant granular flow.

Flows were modeled for a variety of shear speeds and overburden pressures. Results of these simulations show that, although multi-particle collisions do occur with increasing frequency as overburden is increased, they do not have any significant effect on the shear strength of the granular flow. Therefore, this hypothesis is rendered invalid.

ON THE TRANSPORT MECHANISM OF ROCKFALLS AND AVALANCHES

by

Jeffrey Michael Lacy

A thesis submitted in partial fulfillment
of the requirements for the degree

of

Master of Science

in

Engineering Mechanics

MONTANA STATE UNIVERSITY
Bozeman, Montana

April 1989

APPROVAL

of a thesis submitted by

Jeffrey Michael Lacy

This thesis has been read by each member of the thesis committee and has been found to be satisfactory regarding content, English usage, format, citations, bibliographic style, and consistency, and is ready for submission to the College of Graduate Studies.

4/14/89
Date

Jim Dent
Chairperson, Graduate Committee

Approved for the Major Department

4/14/89
Date

Head, Major Department

Approved for the College of Graduate Studies

April 18, 1989
Date

Graduate Dean

STATEMENT OF PERMISSION TO USE

In presenting this thesis in partial fulfillment of the requirements for a master's degree at Montana State University, I agree that the Library shall make it available to borrowers under rules of the Library. Brief quotations from this thesis are allowable without special permission, provided that accurate acknowledgment of source is made.

Permission for extensive quotation from or reproduction of this thesis may be granted by my major professor, or in his absence, by the Dean of Libraries when, in the opinion of either, the proposed use of the material is for scholarly purposes. Any copying or use of the material in this thesis for financial gain shall not be allowed without my written permission.

Signature _____

Date 4/14/89

TABLE OF CONTENTS

TABLE OF CONTENTS--Continued

LIST OF TABLES

LIST OF FIGURES

LIST OF FIGURES--Continued

ABSTRACT

In this thesis, a numerical model of a granular shear flow is developed. This model is two-dimensional and assumes the shearing granules to be identical, smooth, semi-elastic circular disks. The field containing these disks is bounded on the top and bottom by solid blocks of disks with the same properties. The field is bounded on the right and left by periodic boundaries. The top boundary block has an assigned horizontal velocity and overburden mass, and is unconstrained in the vertical direction. The base boundary block is immobile and does not permit scour.

The numerical model is then used to test the hypothesis that, for large overburden pressures, collisions in the shearing region occur involving more than two particles, and that these multi-particle collisions act to reduce the shear strength of the dilatant granular flow.

Flows were modeled for a variety of shear speeds and overburden pressures. Results of these simulations show that, although multi-particle collisions do occur with increasing frequency as overburden is increased, they do not have any significant effect on the shear strength of the granular flow. Therefore, this hypothesis is rendered invalid.

CHAPTER 1

INTRODUCTION

Rockslides and avalanches continue to be studied vigorously by scientists and engineers for very good reason. They are some of the least predictable, most violent, costly, and deadly phenomena Nature has to offer. Extremely large rockfalls and avalanches, though not nearly as common as the smaller ones, deserve extra attention. This is not only due to the amazing catastrophe they can create, but also because of a phenomenon exhibited by them that does not yet have any satisfactory explanation. Simply put, large events move faster and travel further than current accepted knowledge allows. A few examples illustrate the point.

The rockfall of Nevados Huascaran, Peru in 1970 buried the entire town of Yungay, killing more than 18,000 people in about three minutes. Its average velocity was calculated to be about 280 km/hr. To get an idea of the violence of this event, Plafker and Ericksen (1978) calculated from the size of its impact crater that a 65 tonne boulder found in a field later must have been thrown four kilometers, indicating a launch velocity of about 1000 km/hr. On March 6, 1898, near the village of Glarus, Switzerland, a snow avalanche started near the summit of Vorderglarnisch (Fraser, 1978). A little less than a minute later, the Great Glarnisch avalanche had dropped a vertical distance of 5750 feet, and run 4 1/3

miles from its starting point, including 1 1/2 miles of level valley floor. It had an average velocity of 225 mph.

December 27, 1938 saw a huge avalanche sweep down the Shiai-Dani chute in the Kurobe Gorge in northern Japan (Shimuzu et al, 1980). It hit a four story barracks of semi-underground construction, full of sleeping construction crewmen. The third and fourth stories were blown off the rest of the building, launched over a 20 m (66 ft) ridge, and hurled 600 m (well over 1/3 of a mile) across the Gorge. They, and the men inside, were smashed on the far-side wall of the Gorge. The first and second stories were simply crushed. In all, 84 men were killed.

On January 26, 1986 a similar, though probably smaller avalanche hit the village of Maseguchi in Northern Japan, killing thirteen people and destroying eleven homes (Yasue et al, 1987).

On September 11, 1881, a large rockslide started above the village of Elm, in Switzerland (Hsu, 1978). In about forty seconds, it travelled two kilometers, burying the village of Untertal and partly destroying Elm. Its average velocity was estimated at 300 km/hr.

The incredible speeds and runout distances of large events such as these have puzzled researchers and generated much controversy for at least the last three decades. Unfortunately, the very aspect of these phenomena which make them so very interesting -- their extreme violence -- also makes accurate measurements of their internal processes and mechanics virtually impossible. The transport mechanism of the great slides and avalanches, and why they reach such incredible speeds, though much modeled and hypothesized about, remains unknown. Yet these events will continue to occur around the

world in the future as they have in the past, making a better understanding of their behavior not only academically interesting but socially imperative, especially as people move to live and play more and more in the mountainous regions of the world.

In this paper, flow avalanches, which consist mainly of a dense core of flowing snow, are to be distinguished from powder avalanches, which have no such core and resemble more closely in their behavior turbidity currents than rockfalls. For the remainder of this paper the word "avalanche" can be taken to mean "flow avalanche" unless indicated otherwise. Also occasionally rockfalls will be referred to as "sturzstroms" after Hsu (1975) as this seems to be more descriptive of the debris flow aspect we are interested in than "rockfall" or "rockslide".

CHAPTER 2

THE CURRENT STATE OF KNOWLEDGE

Review of Previous Work

Research concerning rockslides and that of avalanches have generally been held separate from each other, although in many respects they are very similar events. Both show the following characteristics regularly, indicating that a similar mechanism drives them both. These characteristics also serve as a guide for researchers, since any hypothesis concerning sturzstoms and large avalanches must take them into account. These are (Davies, 1982):

1. Material in the final deposit is in the same sequential order as it was initially. In material of different colors, there is sometimes distinct longitudinal banding as well.

2. In Sturzstroms, shattered rock fragments remain close together, creating a "three-dimensional jigsaw" effect.

3. In the final deposit there are usually distal ridges, indicating a sudden stop.

4. There is a very strong similarity between deposits of events on earth and those on the moon and Mars, indicating the same mechanism is at work.

5. The size effect: Velocity and runout distance increase with the volume of the event, indicating a corresponding decrease in internal friction.

The serious study of sturzstrom behavior began with Albert Heim and his study of the Elm event mentioned above (Hsu, 1978). He proposed that the debris flowed rather than slid, and was met with some considerable resistance from his peers. In his 1932 paper, he suggested a mechanism for this flow. When any particle has a higher velocity than its forward neighbor, it collides with that neighbor and is not allowed to pass. Energy is transferred to the slower particle through the impact, which in turn collides with another particle. In this way, the sequential order of the flow is preserved and the kinetic energy of the fall is maintained, the only loss of internal energy of the flow being due to inelasticity of particle collisions. This model also satisfies criterion 2, the jigsaw effect, in that fragments of a broken clast would not be able to separate from each other.

In 1965 P. E. Kent proposed an entirely different mechanism. He stated that during the initial fall of rock, air is trapped beneath it. As this air rushes out of the rock mass it fluidizes the particles, thus relieving the interparticle frictional forces and allowing great speed.

Shreve, in 1968, proposed a "hovercraft" mechanism which enjoyed widespread popularity for a time. From his study of the Blackhawk slide, he figured that if a debris flow hit a suitable jump, it would compress a volume of air beneath it, which, due to scale effects, would not be able to escape quickly. The rock mass would then slip on a frictionless air cushion, thus reaching high velocity.

Guest (1971), and Howard (1973) found that rockfall deposits on the moon and Mars were very similar to those being studied on earth, lending serious doubt as to the validity of the air based theories of Kent and Shreve. Then Hsu (1975) and Erismann (1979) discredited the air layer concept completely with excellent arguments, the most

notable being first, the work of Guest and Howard; second, the fact that a volume of air behind a jump is not compressed under a moving "sheet" unless that sheet decelerates considerably (to near stop) while airborne over the volume to be compressed; third, the need for another mechanism to get the rock mass moving fast enough to become airborne from a small jump in the first place; and fourth, that the observed deep gouging of soft earth by sturzstroms is not possible if the flow doesn't actually touch the ground.

Hsu (1975) went on to link Heim's ideas with Bagnold's 1954 work on granular flow in an interstitial fluid. Hsu postulated that highly energetic intergranular dust in a rockfall could serve as Bagnold's interstitial fluid, with or without the presence of air.

From his work on the Kofels slide, Erismann (1979) proposed that high overburden pressures and the heat of friction at the base layer could cause a slide to self-lubricate either by the melting of base layer rock, producing a liquid lubricant, or by dissociation of basal rock (depending on rock composition) to produce a gas-dust lubricant. There is solid evidence for this happening in one case, but lack of evidence in any other leads one to conclude that while this mechanism is thermodynamically feasible, it does not play a great role in the vast majority of large events.

McSaveney (1978) noted that Bagnold's granular shear theory required no interstitial fluid to work, removing any theoretical need for Hsu's interparticle dust.

In 1981, T.R.H. Davies proposed that sturzstroms owe their nature to pure mechanical fluidization. In this model, particles in the flow get enough kinetic energy to become statistically separated, and particle-particle interaction is only through brief impacts. In this state, the flow behaves much like a molecular fluid, and notably, much like Heim proposed in 1932.

In the West, analysis of snow avalanches began with the work of Voellmy in 1955, who proposed that an avalanche could be treated as an open channel, incompressible, steady-state fluid flow. His expressions remain in use in many areas as the foremost calculational tool for the prediction of avalanche danger. However, the method does have limitations. For example, it requires that the point where run-out begins be chosen, rather subjectively, by the analyst. And it requires a choice of a variety of snow and flow parameters including flow density, flow height, and mean deposition depth, which vary with snow and weather conditions, and with the researcher reporting them. There are also some theoretical drawbacks. In the words of LaChapelle and Lang (1980),

> "Formally, The Voellmy method is severely limited because it is invalid for movements with local accelerations, applies to internal snow flow and not the avalanche front, does not describe motion of the airborne dust cloud, and requires the equation of continuity be met. Avalanche observations in the real world, including ours, seldom meet these criteria."

Over the years, several other fluid-based models have been proposed, ranging from Salm's (1966) center of mass motion equations, to Dent and Lang's (1983) biviscous modified Bingham fluid proposal, to the continuum mechanical approach of Norem, Irgens, and Schieldrop (1986).

While these methods can be used to model quite accurately the external features of avalanche events, they rely on such parameters as the kinetic and turbulent coefficients of friction, viscosity, flow height, or locking shear stress, which are impossible to determine for any given event until after it has happened, if at all. Since these parameters must usually be back calculated from the very expressions they are used in, the models are reduced to empirical relationships which may not have any connection with the actual mechanics of the event. Also, because of the wide range of values of these coefficients,

the predictive value of these models is limited.

In 1980, A.I. Mears published a study of 45 avalanches in which he found no correlation at all between the run-out distance and slab height, or between the run-out distance and the slope of either the track or the run-out zone. All three parameters figure prominently in many of the fluid models. He also found that 80 to 90 percent of dry slab avalanche debris consisted of snow fragments larger than 5 cm in diameter. He went on to propose a granular shear flow mechanism such as that studied by Bagnold (1954).

In 1987, Hutter, Szidarovsky, and Yakowitz modeled avalanche flow assuming a granular shear flow mechanism proposed by Jenkins and Savage (1983). They found that it was most realistic to assume that a near-bed layer of material is fluidized, carrying on it the nearly passive load of the bulk of snow. It will be interesting to remember later that the work of Jenkins and Savage, and thus that of Hutter et al, is based on their explicit assumption that particle interaction in the fluidized region is strictly through binary collisions.

Currently, researchers in both the fields of rockfalls and snow avalanches are coming to embrace the concept of near-bed fluidization as the major transport mechanism. In this model, as a falling mass of rock or snow gains velocity, granules or clasts near the base of the flow, where the shear rate is highest, gain enough energy to separate, dilating that layer. The material above this fluidized layer is carried passively and deforms slowly relative to the highly activated shear region. The expanded base layer has very little shear strength, allowing the low observed apparent coefficient of friction of large events. This model satisfies the observed behavior characteristics as follows.

Sequential order of the material in the final deposit is maintained since the bulk of the material is carried relatively passively by the highly activated shear layer. The shearing layer entrains material from the leading edge of the flow and deposits it at the rear, accounting for the thin smear on the bottom of the final deposit noted by Dent (1982).

The "three dimensional jigsaw" effect is also due to the fact of the slowly deforming bulk of the flow. Since there is little or no turbulence in the majority of the material, clasts broken in the original fall will remain close together during the runout.

Lateral ridges in the distal regions of the final deposit form due to the collapse of the dilated shear layer. As the flow loses speed in the run-out, the front-most regions of the dilatant base layer will lose enough energy to collapse, suddenly increasing friction forces and decelerating quite rapidly. Material behind the collapsed region will collide with it and try to ride up over the slower material before losing momentum itself, causing a series of lateral ridges in the distal areas of the deposit.

The similarity of terrestrial events to those on the moon and Mars arises because all that is required for this mechanism to work-- gravity and some bulk material to flow-- is available at all three sites.

The size effect, wherein velocity and runout distance increase with the volume of the event, is not necessarily explained by this model. It appears that although the model is basically correct, there is an additional mechanism at work within the shearing region which has not yet been accounted for.

The Problem

The size effect observed in large avalanches and sturzstroms is not explained effectively by the current fluidized base layer theory. Direct radar measurements of avalanche velocities by Gubler (1987) and observations by many others leave no doubt about the veracity of this phenomenon. The loss of internal energy of both sturzstoms and avalanches decreases as the volume of the event increases, yielding higher velocities and longer run-out distances for large events.

Although a dilatant base layer does reduce the apparent friction of a granular flow, it should not, according to present knowledge, do so in the manner observed. As the mass of a flow increases, there should be some jump in velocity as the critical mass for bed fluidization is reached. Then as mass is added, the dilatant layer should be compressed, shortening the mean free path of the fluidized particles, and increasing the shear strength of the layer, slowing the flow. McSaveney (1978) stated the problem like this.

> "With increasing thickness of avalanche, the mean free path of the clasts shortens, and hence the frequency of collisions increases with thickness as well as with number of clasts. Large, thick avalanches might thus be expected to lose energy more rapidly than smaller, thinner ones, and thus have higher internal friction."

Currently, a mechanism that would resolve this contradiction between expectation and observation is being sought. Dent, in 1986, proposed the following hypothesis:

As a fluidized bed is compressed by increasing overburden, collisions between particles cease to be purely binary, and multiple collisions begin to occur. These multiple collisions form, for the briefest of moments, chains of particles, or microstructures, in the layer which have high axial strength and low or negligible shear strength. Cumulatively, these microstructures could help support the overburden pressure without much affecting

the shear strength of the layer, thus effectively reducing the ratio of shear to normal stress and reducing the apparent friction of the overall event. To state this concisely, this hypothesis predicts that

1. A fluidized bed compresses as overburden is added.
2. This compression causes multiple-contact microstructures to form.
3. These micro structures present a lower ratio of shear resistance/normal force than do binary collisions alone.
4. These structures form frequently enough to reduce noticeably the overall shear ratio, and thus reduce the apparent friction of the flow.

The purpose of this research is to test the predictions of this hypothesis and discover if this is a viable explanation for the size effect.

CHAPTER 3

INVESTIGATION

The investigation of this hypothesis was a numerical (computer) simulation of a shearing system of particles. The experiment was designed both to observe whether microstructure chains actually do form, and to measure their effect on the shearing system as a whole.

Numerical Simulation

The first phase of research was to build a computer simulation of the basal shear layer. The model is a two dimensional field of disks, bounded on the bottom by a row of immovable disks and on the top by a row of disks with an assigned horizontal velocity and overburden mass. At the left and right hand edges of the field there are periodic boundaries, meaning simply that whatever exits the field on one side will reenter on the other, with the same altitude and velocity. All particles are assigned a diameter, mass, hardness (spring coefficient), and elasticity (coefficient of restitution).

The simulation follows the exact paths of all the disks in the field, calculating the position, velocity, and acceleration of each over small time increments. Accelerations only occur when a particle is in contact with any other. This simulation is different from that of Hutter et al (1987) and the grain flow simulation of Campbell (1982) in that those

models assumed only binary collisions between particles and simply calculated the results of each contact, where this model follows the true path of particles, allowing any number particles to contact at once.

The Code

The following section is a detailed description of the numerical simulation code. SNOFLO was written by the author in June, 1988 in Fortran on a VAX/VMS network system.

The code will be discussed by its sections in the following order:

1. Data and parameter input
2. Run initialization
3. Virtual elements and periodic boundaries
4. Contact mechanics
5. Contact parameter flags
6. Impact subroutine
7. Time jumping subroutines
8. Positions, velocities and forces
9. Output and graphics
10. Simulation accuracy and discussion

This order is used because it follows the flow of the code itself. A copy of the code is listed in Appendix A for more rigorous inspection.

Data Input and Parameters

Run parameters are read from the data file CNTRL.DAT. Reads are unformatted --only the parameter order is important. The parameters, in the order they appear in CNTRL.DAT are:

RESTRT,GRAPH
K1, K2, D, M, G, MTOP
NHT, NWID, TWID, VXT
STEP, LOOP, TIME

Where the first row contains I/O flags; the second the physical properties of the material chosen, in the desired units; the third row contains array and field building information; and the fourth has time parameters. Each parameter and its function will be discussed in turn.

The RESTRT flag indicates whether or not the ensuing run is new or the continuation of an old one. If RESTRT equals 1, particle positions and velocities, along with the elapsed time and total number of cycles, are read from a formatted file RESTART.DAT, which was created by the run which is to be restarted. A new restart file is created at every output interval during a run. This ensures that in the event of an accidental abort or interruption very little time will be wasted recovering old ground. If RESTRT equals 0 a brand new array of particles is created.

GRAPH is a graphics flag. If this is set to one, then at each output interval a formatted file PIC.DAT is created, into which is fed the position of every particle (real or virtual) that is either within or is touching the field boundaries. The subroutine PICTURE is then called, which reads the particle positions and employs a series of DISSPLA commands to create a META.DAT graphics file. This allows "pictures" of the particle field to be taken at desired intervals. This visual information can be especially useful in helping

the observer to understand how the simulation is progressing. With properly timed graphics intervals, one may use a movie camera to take single frame pictures of a run as it progresses, creating an animated film of the simulated shear region. This was done, and although it is a very time consuming process, the resulting film yields valuable information about the nature of the fluidized system of particles.

K1 and K2 are the spring constants of the particles and represent their "hardness." In a binary collision K1 is the approach constant, while K2 is the retreat constant. The ratio K1/K2 is in real time the coefficient of restitution of the material **e**. See Figure 1.

Figure 1

Contact Force and the Overlap Delta

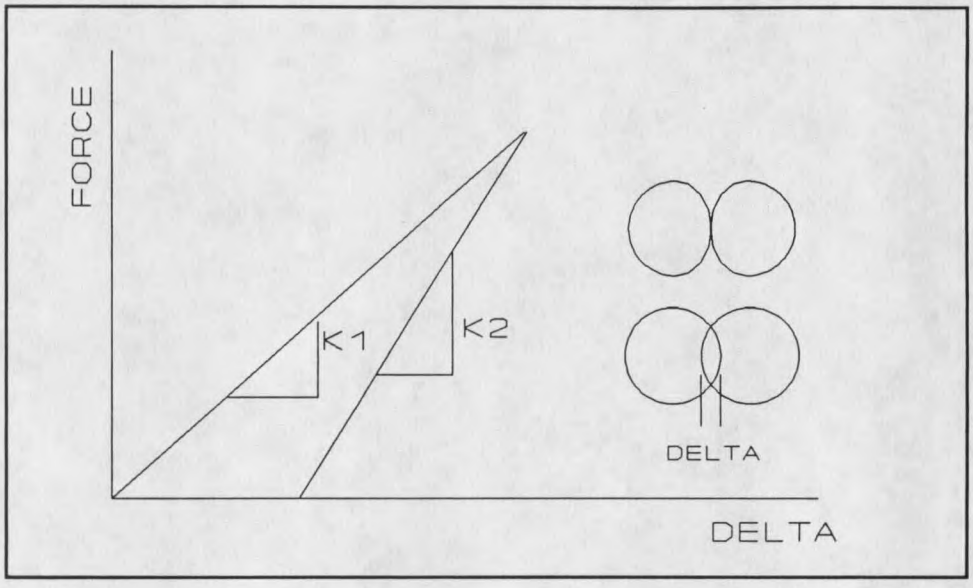

In the numerical simulation, time is not continuous, but is discretized into finite steps. This causes the ratio K1/K2 to become less than the actual coefficient of restitution. The amount of variation is directly dependent on the size of the time step chosen. To find K1/K2 for a desired **e**, a field was set up such that two particles could collide without

interference. Then the ratio K1/K2 was adjusted to achieve the desired rebound velocities calculated from the desired coefficient of restitution. It was found that for a time step of 10^{-7} sec, and a coefficient of restitution of 0.7 the ratio of K1/K2 was 0.45. It was found that the coefficient of restitution is stable for impact velocities spanning four orders of magnitude. The relationship between K1, K2, and DELNOT becomes more complicated during multiple collisions. This event will be discussed in detail later.

The diameter and mass of the particles are D and M, respectively. In this model, all particles are of uniform size and mass. While this gives quite useful results, it would be interesting to see the results of a similar model with randomly sized particles. This is recommended for further investigation.

G is the gravitational acceleration, scaled to whatever system of units the investigator has chosen. Gravity does not act on the free particles in the array. It only acts on the upper block of particles. This upper block represents the bottom surface of the slowly deforming overburden load. Hence it is assigned mass MTOP, which represents the mass of the snow or rock above the field. To find overburden pressure, one must find the force MTOP*G, and divide by the field area TWID*D^2.

The next row of parameters define the size of the array to be used and the width of the field to which it is confined. The free particles are initialized in a rectangular matrix. NHT gives the number of rows of the matrix, and NWID gives the number of columns. TWID is the number of particles in both the top and bottom boundary blocks and hence also gives the width of the field in diameter lengths. After initialization, the field is set up as in Figure 2.

Figure 2

Shear Field Initialization

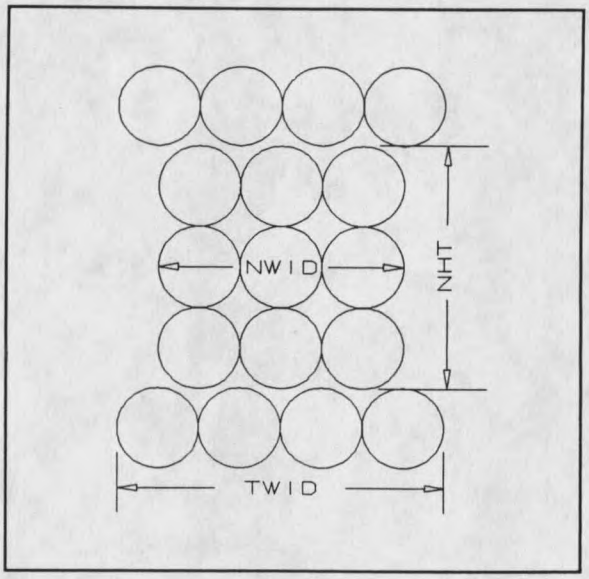

VXT is the assigned horizontal velocity of the top block. This remains constant, although the vertical position and vertical velocity are free to change.

The last line of CNTRL.DAT gives the time parameters of the code. STEP is the size of the time increment to be used while calculating collision results. This may be made small at expense of much CPU time, or larger at the expense of accuracy. For this work a time step of 10^{-7} was used and yielded good results. LOOP is the output time interval. At the end of each interval, all output files are updated and graphics are created. TIME is time interval for which the simulation is to run. Although this can be made arbitrarily large so that runs may be aborted when the investigator chooses, this is not recommended. Without a logical stop, all graphics files will be lost. Also TIME should be kept small until

an investigator is familiar with the properties of the simulation--one second of flow time averages 10 to 13 hours of CPU time on the VAX.

Run Initialization

After the run parameters have been defined, the particle array is built as described previously. Each particle is assigned a scalar identification number and an initial velocity. The horizontal velocities vary linearly from the bottom to the top of the array, while vertical velocities are small and semi-random. The initial velocities serve the purpose of quickly breaking up the initial rectangular particle matrix into a random field, instead of wasting computer time to let the effects of the top block filter down through the array.

If the run is a restart, positions and velocities are read directly, and this step is bypassed.

Virtual Elements and Periodic Boundaries

The next step is the creation of a set of virtual particles, one for each real moving particle, in a field adjacent to the left border of the real field. Each virtual particle is assigned an identification number the negative of that of its corresponding real particle. At each time increment each virtual particle is assigned the velocity and position of its "master." Thus the assembled real and virtual fields are as shown in Figure 3.

Figure 3

Virtual Particles and the Virtual Field

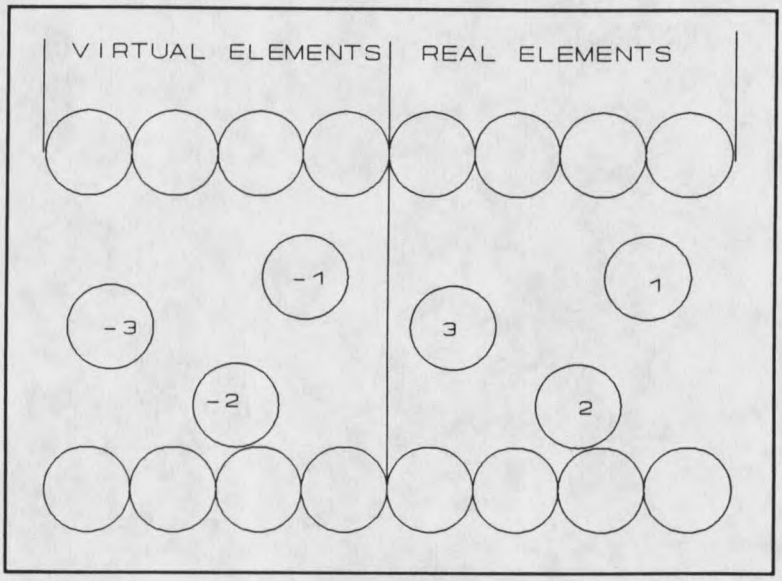

Interactions between negative particles are not calculated, since that would merely be repetition of what was already done in the real field.

These virtual particles don't come into play until a real particle starts to move across a boundary, as in Figure 4. Here, as soon as the center of particle (1) gets to within 1/2 of a diameter from the boundary, its edge is on or across the boundary line. Since now particle (-1) is now partly in the real field, it may interact with any other particle in the field, such as particle (2), as is shown. Any forces the virtual particle feels are assigned directly to its master. Thus the particle (1) in Figure 4 is in contact with both particle (2) and particle (3).

Figure 4

Particle Contacts Across a Periodic Boundary

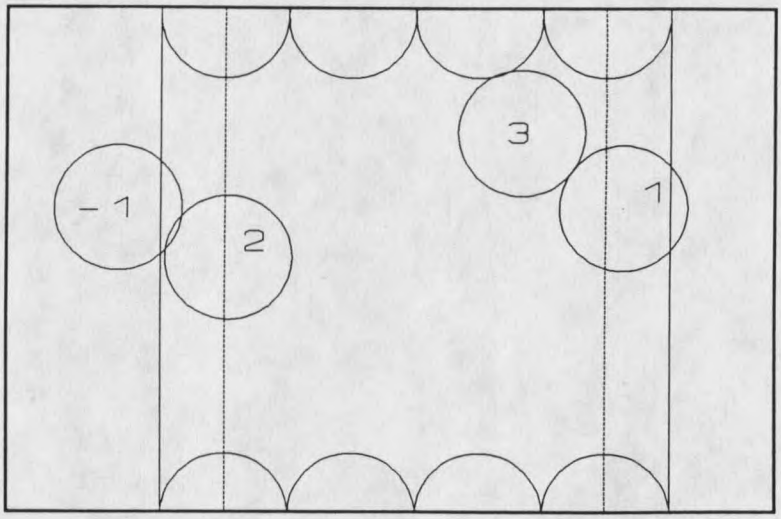

In this way both the element and its virtual may interact in the field while some part (but not all) of the real element is within the boundaries. The transition as a particle crosses the right boundary is shown in Figure 5.

Figure 5

Particle Moving Through the Right Periodic Boundary

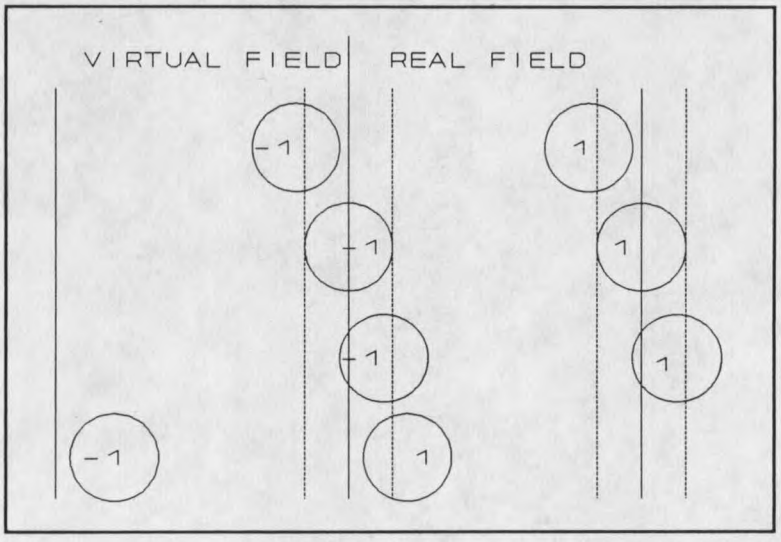

Transitions across the left boundary are similar, but slightly different. When a real particle touches the left boundary, both it and its virtual are shifted one field length to the right, placing the real particle on the right border and the virtual on the left. See Figure 6 for illustration.

Figure 6

Particle Passing Through the Left Periodic Boundary

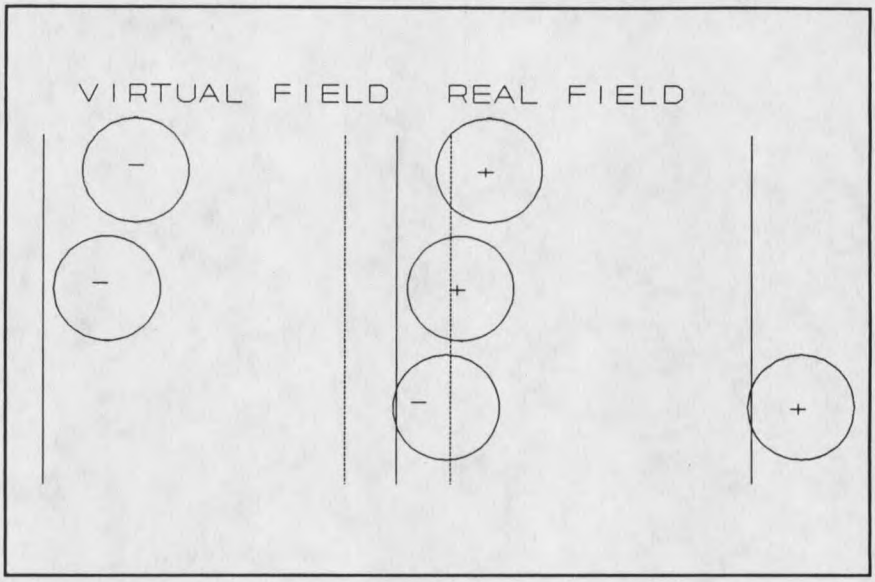

In this manner the simulation is given periodic boundary conditions, meaning that the flow repeats itself spatially every TWID diameter lengths.

Contact Mechanics

The next step is the calculation of the distances between particles and the calculation of contact parameters for colliding pairs. First, though, it would be best to discuss the mechanics of the particle collisions to lend some meaning to those parameters.

In a binary collision, the repulsive force between the two particles follows a path such as that shown in Figure 7. As the elements approach each other and the overlap between them increases, the force increases along path C1 (with slope K1) until it reaches a maximum when the particles are stationary relative to each other. Then as the particles separate, the force decreases, along path C2 (with slope K2) to point DELNOT. At this point the repulsive force between the particles is zero even though there is still some overlap. Thus DELNOT can be thought of as the one dimensional plastic deformation of the particles resulting from their collision. Now the energy absorbed elastically by the particles on their approach is the area under the C1 curve, while the energy released during the separation is the area under C2; the energy of deformation thus being the difference. The coefficient of restitution **e** is then the ratio A2/A1, or K1/K2.

Figure 7

Contact Force vs. Overlap
for a
Binary Collision

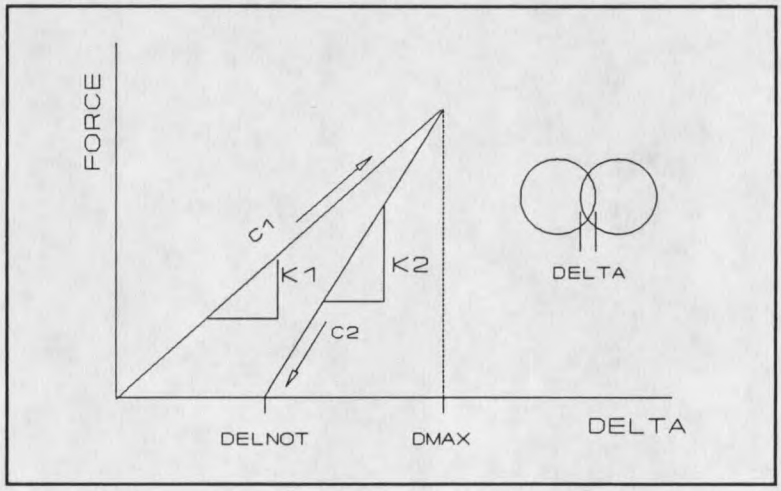

The mechanics of a multiple collision are somewhat more complicated. Consider Figure 8, wherein two particles collide and are starting to move away from one another when a third particle strikes one of the colliding pair. We will consider only the path of the repulsive force between the original two particles.

Figure 8

Contact Force vs. Particle Overlap
for a
Multi-Particle Collision

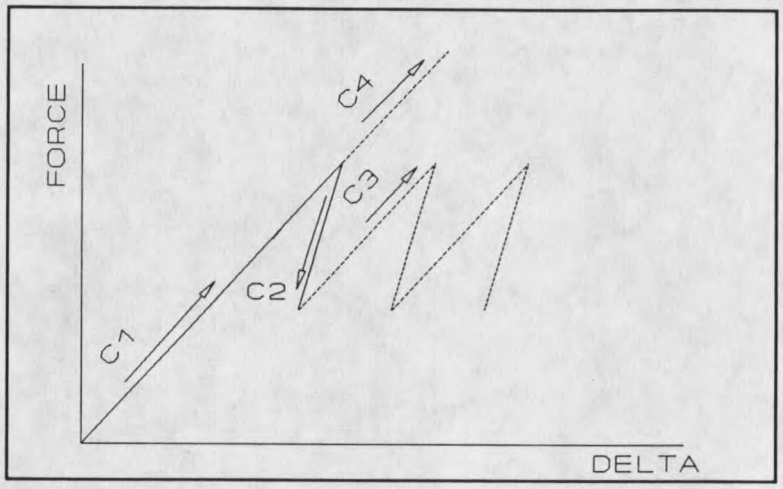

When the two particles first collide, the force follows path C1 as Delta increases. After they have attained a maximum overlap, they begin to separate, following path C2, when one is struck by a third particle driving the original two together again. If the particles' stiffnesses are governed only by whether they are in approach or retreat, then the spring constant is chosen as K1, and the force follows path C3. It is easily seen then that by the time the repulsive force reaches its previous maximum, the overlap between the particles is significantly larger than it was originally. Thus the particles have moved closer together without an attending increase in repulsion. It is easily imagined that in a highly energetic

compressed field, such a pair might suffer a series of several of these impacts, until both particles are occupying the same space with no force between them. This corresponds to real snow or dust particles absorbing so much impact energy that they are broken in several smaller pieces. However, these simulated particles are not capable of such behavior and would merely coalesce.

To avoid such behavior, a third parameter is added to the repulsive force function. This is the maximum overlap condition. The spring force is then specified not to be K1 unless the particles are approaching and their overlap is the maximum for this collision. Thus, upon the impact of the third particle, the force would retrace path C2 until the overlap equaled the original maximum again, and would then move up path C4 to its new maximum. In this manner the relationship between the repulsive force and the overlap is kept independent of its path history, and particles are not allowed to merge.

Contact Parameter Flags

Now in the main program loop, which is repeated for each time increment, the program first calculates the separation parameters S, SLD, and SLDR. S is the new distance between particle centers; SLD is the S of the previous time step; and SLDR is the SLD of the previous time step. These are found for every pair of particles currently eligible to interact in the field as discussed in the section on periodic boundaries. Those particle pairs which have separations less than a diameter are now examined for possible contact. If S is less than SLD, the particles are coming together and the approach flag is set. If SLD is less than S, then the particles are separating. Additionally, if SLD is less than SLDR, the previous overlap was a maximum and DELNOT, the plastic deformation, may be evaluated. DELTA, the effective overlap of the pair, is then a diameter length less

the separation S, less the plastic deformation, DELNOT. If DELTA is positive, then there is contact, and the contact flags are set. Finally DELTA is compared to the maximum overlap, and the DMAX flag is set.

From this point, there is a branch in the code. At any given time, the chances of a collision occurring are quite a bit smaller than that of nothing happening at all. Since the time increment is made quite small to smooth out collision responses, stepping forward at this pace between contacts would be extremely time consuming and prohibitively expensive. Therefore, if there are found to be no collisions occurring, control is given to the subroutines TYMJUMP and TIMER, which compute the time until the next collision for every pair of particles, find the minimum, and jump to there. If collisions are occurring, control is given to the subroutine IMPACT, which computes the accelerations of colliding particles. Continuing along our original train of thought, we will assume there is a pair of particles in contact, and examine IMPACT first.

Subroutine IMPACT

After the contact flags have been set, the subroutine IMPACT is called for those particle pairs with a non-zero flag.

The first step is to determine which particle is to the right of the other and determine the impact angle. This allows the calculated impact values to be decomposed into Cartesian components. The right-most particle must be determined so that the impact angle is unambiguous. Next, a spring constant is chosen according to the values of the approach flag and the maximum overlap flag for the pair. Finally the particle accelerations (forces) are calculated, and control is returned to the main program.

Figure 9

Impact Angle Theta

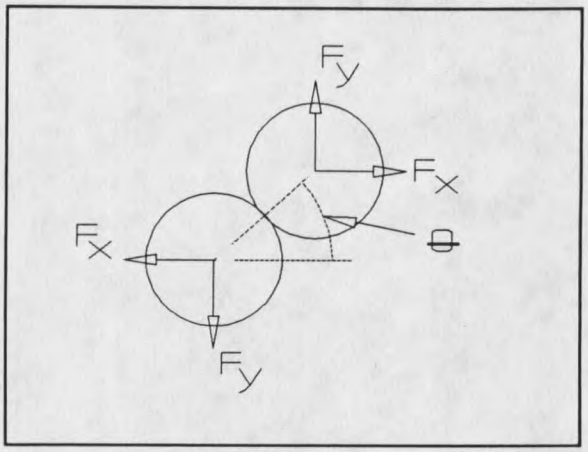

Subroutines TYMJUMP and TIMER

In the event that the evaluation of contact flags reveals that no collisions are taking place, TYMJUMP and TIMER are called. TYMJUMP calculates the length of time until the next collision for every particle pair in the field, except those which are both virtual elements. This is done by solving for the roots of the equation and rejecting negative roots. Note that zero roots are not rejected. Of each pair of roots, the smallest non-negative root is placed in a two-dimensional array TTI (time-to-impact) to be evaluated by the subroutine TIMER.

TIMER compares the elements of the TTI array and passes the smallest one back to the main program.

Back in the main program, the next time step is chosen. If the calculated time jump U is less than STEP (the normal time increment) then the next time step is STEP. If U

is so large that it would jump past an output interval it is reduced to just meet the output interval. Otherwise the simulation is stepped forward by the calculated jump U.

Positions, Velocities, and Forces

Finally, the positions and velocities of the particles may be updated, and the forces on the boundary layer are found.

For free particles, the new position and velocity are calculated using the simple laws of motion and the acceleration and time increment from IMPACT and TIMER. To find the vertical position and velocity of the top block of particles, the forces on the individual elements in the block are summed yielding a total normal force, FYT, and horizontal shear force FXT. Then the vertical acceleration of the top block is the vertical force on it, FYT, divided by its mass, MTOP, less the acceleration of gravity G. Since the simulation is driven by shear velocity, the horizontal velocity of the top block remains constant.

To time average desired variables, each is multiplied by the current time step and added to a sum. At the output interval, the sum will be divided by the total time in the interval, yielding the average.

The ratio of the shear and normal force, S/N is the main object of interest in this simulation, and deserves a little more discussion. At each time step FXT and FYT are time weighted and summed separately. If a multiple contact is occurring (MULTI=1) then they are also summed to multiple contact shear variables. Note that they are not first divided and then ratio averaged. This would be invalid since times with no contact at the top layer would yield a zero ratio, which is the same result as a perfectly vertical collision with no shear component, thus giving erroneous results. At the output interval, the sums are divided and both the total shear ratio and multi-contact shear ratio are evaluated.

Output and Graphics

At the end of each selected time interval LOOP, SNOFLO writes data to the data file SNO.DAT, to the screen or .LOG file, to the RESTART.DAT file, and, if graphics are on, to PIC.DAT. Data written to the default file and SNO.DAT are identical and consist of the cycle number, total shear ratio, multiple contact shear ratio, the fraction of time there were contacts, the fraction of time there were multiple contacts, the total elapsed time of the run, and the current time increment. Beneath this are listed the average positions, velocities, and accelerations of all moving particles in the field.

Information written to RESTART.DAT includes the field dimensions, number of particles, the cycle number, elapsed time, and the exact positions and velocities of the particles.

If the graphics flag GRAPH equals one, a picture of the field is taken as described previously.

Simulation Accuracy and Discussion

In any numerical modeling problem, various simplifications and assumptions must be made to make the problem not just easier, but possible to model. This case is no exception. The problem then becomes whether or not these simplifications are justifiable when compared to their adverse affect on the results produced by the model. Usually, this kind of problem reduction results in a model which has poor or non-physical behavior in some aspects or processes.

In this section several of the assumptions built into the SNOFLO model will be listed, and the impact each of these has on the numerical results as a whole will be briefly discussed.

The assumptions in SNOFLO can be divided in two groups: assumptions about the particle characteristics, and assumptions about the medium or environment they interact in. Assumptions concerning particle characteristics are:

1. They are frictionless.
2. They are all of uniform size and shape (round).
3. They are perfectly "tough."

Together, the lack of friction, uniformity of size, and circular shape simplify greatly the mechanics of a collision. Zero friction eliminates the effects of spin, making all collision forces diametrical. A circular shape is necessary if particle orientation (which cannot change without spin) is not to play a factor in the overall results. Size uniformity was chosen because while it simplifies the problem, it is also easier to corroborate with real shear test devices. The "perfectly tough" assumption means that however much collision energy the particles absorb, they won't break. This ties in closely with the uniform size assumption.

These assumptions, especially that of zero friction, will result in a drop in both the total shear ratio and the multiple contact shear ratio. The shape, size, and toughness restrictions should not make any further noticeable reduction in accuracy.

Simplifications in SNOFLO of the environment include:

1. Flow is two dimensional.
2. Flow is spatially periodic.
3. The fluidized bed is very shallow.
4. No particles are either entrained into or lost from the fluidized layer.
5. Gravity does not act on the fluidized layer.

The model was made two-dimensional for two reasons. First, the computational effort required for a three dimensional analysis, and hence computer time and cost, would be enormous and prohibitive. Second, data analysis and verification would be quite a bit more difficult. The two-dimension simplification does have a side-effect. For particles to form a micro-structure they are always lined up in the third dimension and need only to align themselves in the other two. This makes the likelihood of such a chain forming higher than it is in reality.

The next three simplifications--that the flow is periodic, shallow and doesn't entrain more particles at high energy levels--are again due to limited computational resources. Each allows fewer particles and hence fewer degrees of freedom to be modelled. The periodic flow condition is only valid for steady state flow and creates inaccuracies at low shear speeds, where the flow regime is unstable. A shallow fluidized bed is probably an accurate assumption at low shear speeds, however as a fluidized bed gains more energy as the shear speed increases, it will gouge material from the base layer, entraining more particles, becoming deeper, and reducing its strain rate. Thus data for very high shear speeds is not entirely to be trusted.

Finally, gravity is not applied to the freely moving particles in the field. This might have some effect if paths between collisions were longer and the velocities of the particles were a lot lower. As it is, the error introduced here is negligible.

Experimental Procedure

For an initial test of the predictions of the microstructure hypothesis, SNOFLO was employed to simulate flow at varied shear speeds and overburden pressures.

All simulations used the same field dimensions and physical properties. The field was four particles in width, and contained nine free particles. Each particle was 1 mm in diameter, and had a mass of .0005 g. The particle stiffness (K1) was 45000 N/m and the coefficient of restitution was 0.7.

Three series of runs were made for constant overburden and varied shear speed. Overburden pressures used were 2000 Pa, 15,000 Pa, and 32,000 Pa. Shear speeds were varied from 500 diameters/second to 10,000 diameters/second.

One series of runs was made for a constant shear speed of 5000 d/s. Overburden pressure for this series varied from 2000 Pa to 40,000 Pa.

Each run in a series was made at constant overburden and shear speed, and was modelled for one second of flow. The resulting data was then averaged for half-second intervals. Each run took about 10-13 hours of CPU time on the VAX/VMS 8550 machine. Results of each series of runs were used to create various plots descriptive of the behavior of the flow. These plots and a discussion of them follows in Chapter 4.

CHAPTER 4

RESULTS AND CONCLUSIONS

Results

In this section, the results of the numerical simulation will be discussed using graphs of the data generated by the model. Since this is more a qualitative than a quantitative analysis, all data points are included irrespective of their fit, and no curves have been fit to the data. Hence the discussion will focus more on general trends in the behavior of the shearing region as different parameters are varied. Discussion of the results will begin with a comparison to previous work to validate the model itself. Then the behavior of the shear flow will be analyzed to determine the validity of the microstructure hypothesis.

To check the validity of the SNOFLO model, its results for the stress ratio versus shear speed will be compared to the same results generated by previous investigators. This data is used as the tool for comparison because it is commonly reported and is straight forward to compare. The stress ratio S/N is the ratio of the horizontal (flow resisting) force to the normal (dilating) force exerted on the top block by the particles in the shearing region, summed and averaged over the total time of flow.

The first three plots (Figures 10, 11, and 12) were generated from data produced by SNOFLO, and show the stress ratio versus the shear velocity for constant overburden loads of 2, 15, and 32 kPa respectively. The shear speed in these plots is varied from 500

to 10,000 diameters per second (d/s). Recall that the coefficient of restitution for these particles is 0.7. Figure 13 shows a plot of the stress ratio versus shear speed calculated by Dent (1988) from the theory developed by Richman and Chou (1986). In this plot, particles are assumed to be round, frictionless, and 1 mm in diameter. They have a coefficient of restitution of .95. The overburden load is 0.1 kPa.

Figure 14 shows the results of Dent's (1986) quasi-two-dimensional model. These particles have friction and a coefficient of restitution of 0.8, while the other particle parameters are the same as in Figure 13.

The next three plots, Figures 15 through 17, were created by Dent (1988) from data produced by Hanes and Inman (1985), Savage and Sayed (1984) and Bridgwater (1972) respectively. Data from all three investigations was collected from annular shear cell experiments. To explain, an annular shear cell is a device consisting of a cylindrical trough and a cylindrical ring which just fits inside the trough. The material to be sheared is placed in the trough and the top ring is placed on top of this material. The top ring is then spun relative to the trough, shearing the material between them. Normal pressure is regulated by weighting the top ring, while shear speed is regulated by its angular velocity (spin rate). Shear force can then be measured from the torque applied by the shearing material to the stationary trough. For further illustration and discussion of this device, see Savage and Sayed (1984).

Hanes and Inman (Figure 15) used 1 mm glass beads at overburden pressures of .336 kPa and 1.054 kPa. The results shown for Savage and Sayed (1984) are for 1 mm polystyrene beads a normal pressures of .9 kPa and 1.05 kPa. Bridgwater's (1972) results are for 2 mm glass beads, with reported normal pressures of .62, 1.46, 6.05, and 16.7 kPa.

It is immediately apparent that the parameters used in the investigations presented here have significant differences. Particle characteristics such as size, hardness, elasticity, and roughness all vary. Combined with the probable differences present in experimental procedure, this makes a quantitative comparison of these results impossible. It is possible, however, to compare them in a qualitative manner. A comparison of the shape of the data curves produced by SNOFLO with the shapes of other data curves should be sufficient to determine whether or not the model behaves in a manner consistent with behavior previously observed.

Notice that both the theory of Richman and Chou (Figure 13) and the numerical model of Dent (Figure 14) predict a drop in the stress ratio at extremely low speeds, followed by a rise in the stress ratio at higher speeds. This initial drop in the stress ratio is due to the transition of the shearing region from a compact state to dilatant state. This behavior does not show up in the other plots since speeds reported are above this transition level.

Comparing the results of SNOFLO with the results of the other investigators, one notes two points of strong correlation. First, the curves have generally the same shape; second, the way the curves change as overburden is increased is consistent.

The stress ratio in all the data plotted starts at an initially low value (after dilation) and rises with increasing shear speed. The SNOFLO data indicates that the stress ratio reaches a maximum at some speed, and then remains fairly constant after that. Although none of the other plots are carried out to correspondingly high shear speeds, the asymptotic shape of both Figures 13 and 14, and the shape of the data in both Figures 15 and 16

make it seem likely that these would behave in the same fashion. Thus the shapes of the curves from SNOFLO are consistent with the others.

The second point of correlation is that the curves respond similarly to increases in the normal load. Reviewing Figures 10 through 12, one sees that as the normal pressure is increased from 2 kPa in Figure 10 to 32 kPa in Figure 12, the response of the stress ratio to the shear speed is decreased. In other words, as the overburden increases the slope of the stress ratio decreases. This same behavior is apparent in Figures 15 through 17. Curves for higher overburden values tend to be lower and flatter than those for low overburdens. This behavior is significant and will be discussed in more detail later.

This comparison of various results also reveals a weakness in the SNOFLO simulation, even though it was anticipated before. The zero friction assumption yields a stress ratio significantly lower than that given by physical testing. Though this has little effect on the results being sought currently, care should be taken if this code is to be used for other purposes.

This analysis yields some useful conclusions about the validity of the SNOFLO numerical model. First, the quantitative results of any granular shear model, physical or numerical, are very sensitive to variations in the material parameters involved. This is evident from the wide range of values obtained by different investigators. Second, friction does play a large role in the shear strength of the fluidized region, even at high shear speeds where the flow is statistically separated. Third, the qualitative behavior of the granular shear flow is relatively insensitive to both the material properties and to changes in particle roughness. This conclusion is reasonable since curve shapes (and therefore the flow behavior) remained consistent for all the different experiments discussed.

Given these conclusions, and the overall consistency of the SNOFLO results with those of previous investigations, it may be concluded that this model yields valid results, and that data generated by it may be accepted as at least a first approximation of the behavior of a real granular shear flow.

Figure 10

Stress Ratio S/N vs. Shear Velocity at 2 kPa

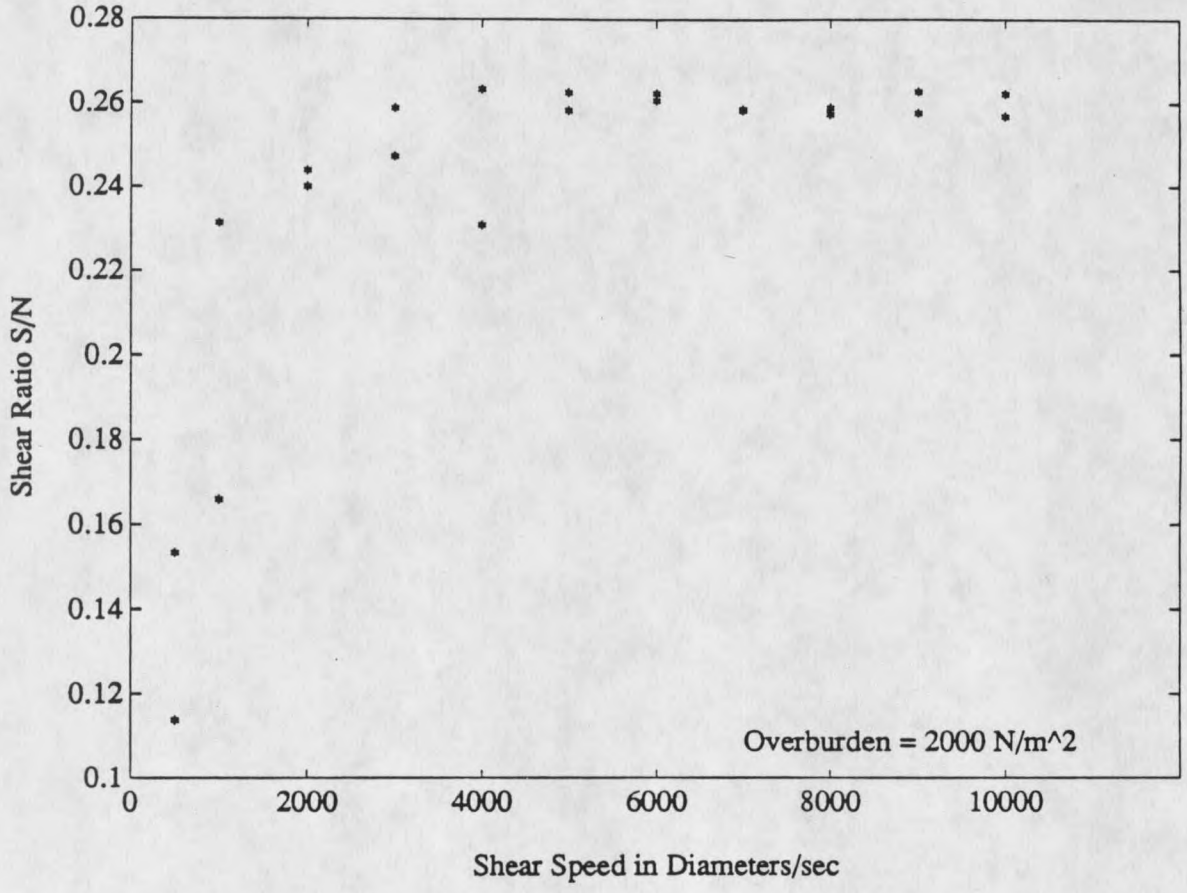

Figure 11

Stress Ratio S/N vs. Shear Velocity at 15 kPa

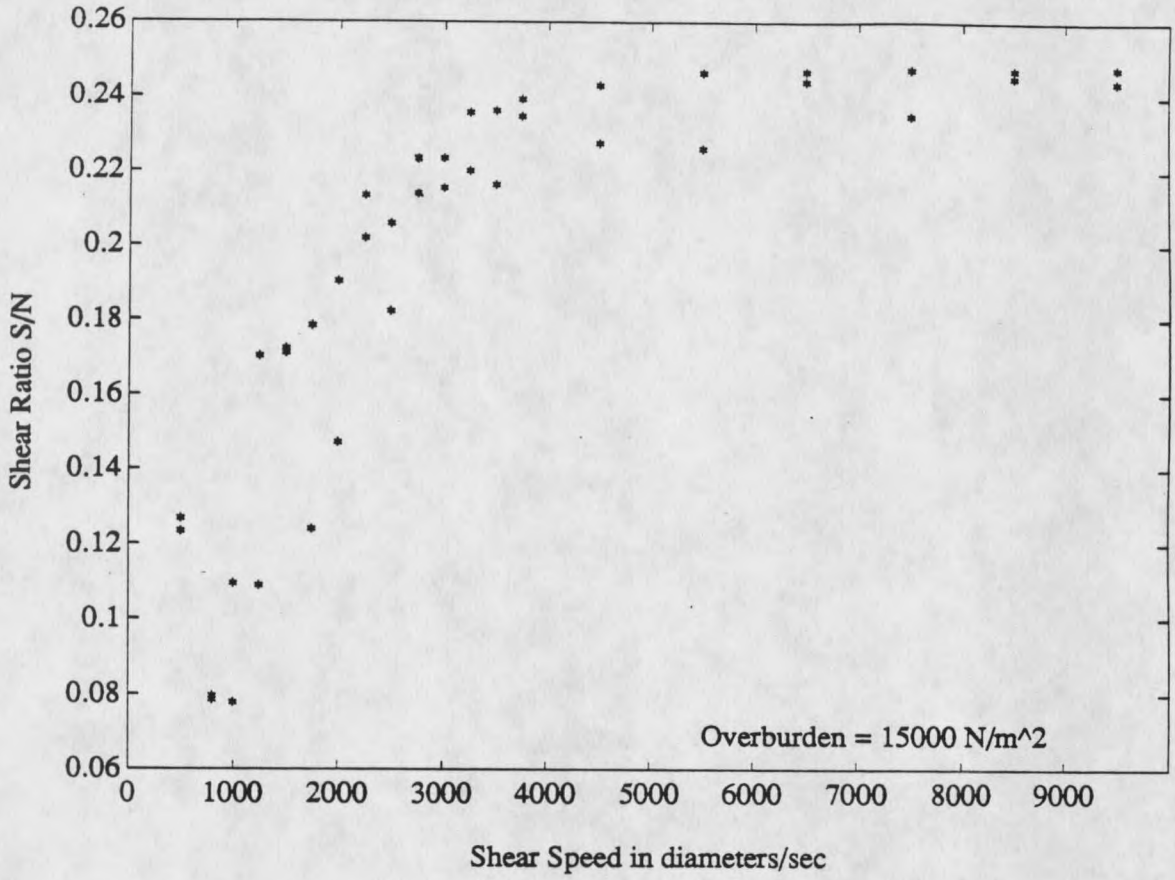

Figure 12

Stress Ratio S/N vs. Shear Velocity at 32 kPa

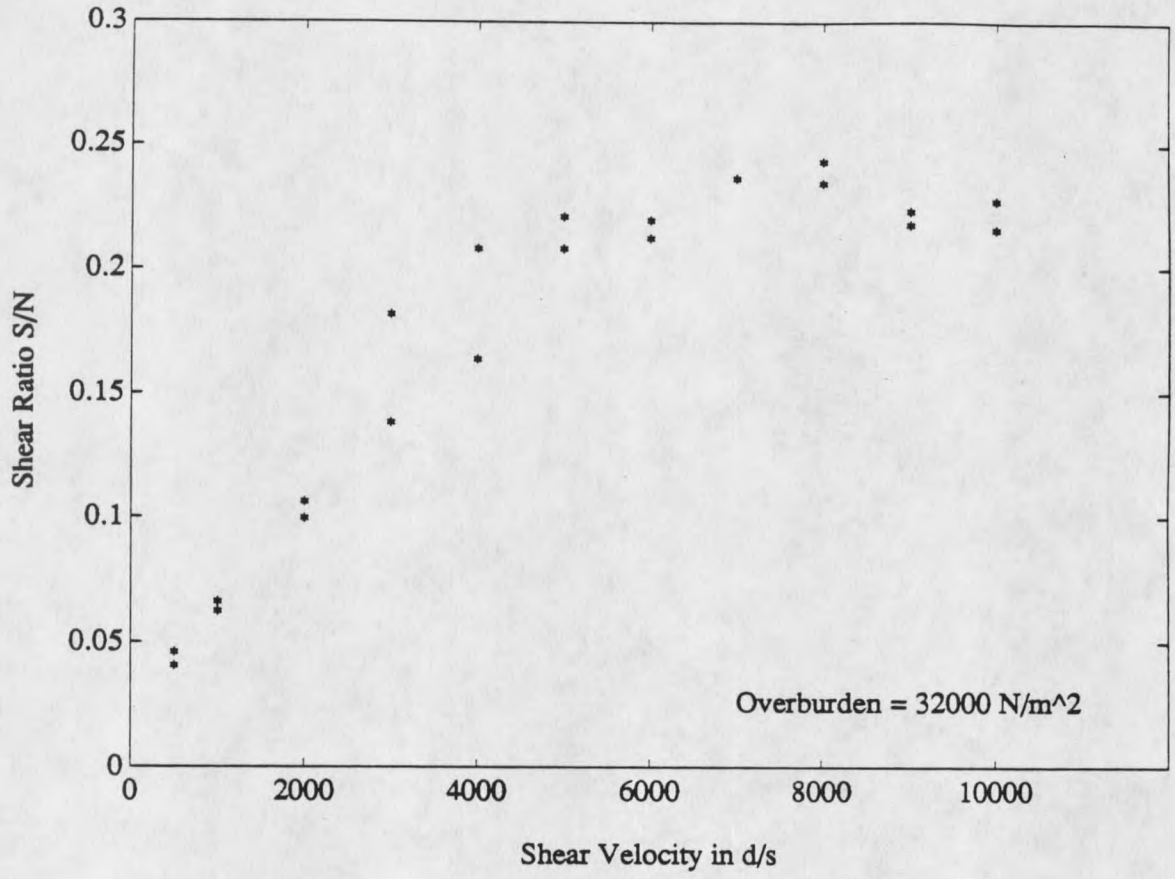

Figure 13

Stress Ratio vs. Shear Velocity Derived from Theory of Richman and Chou as Reported by Dent

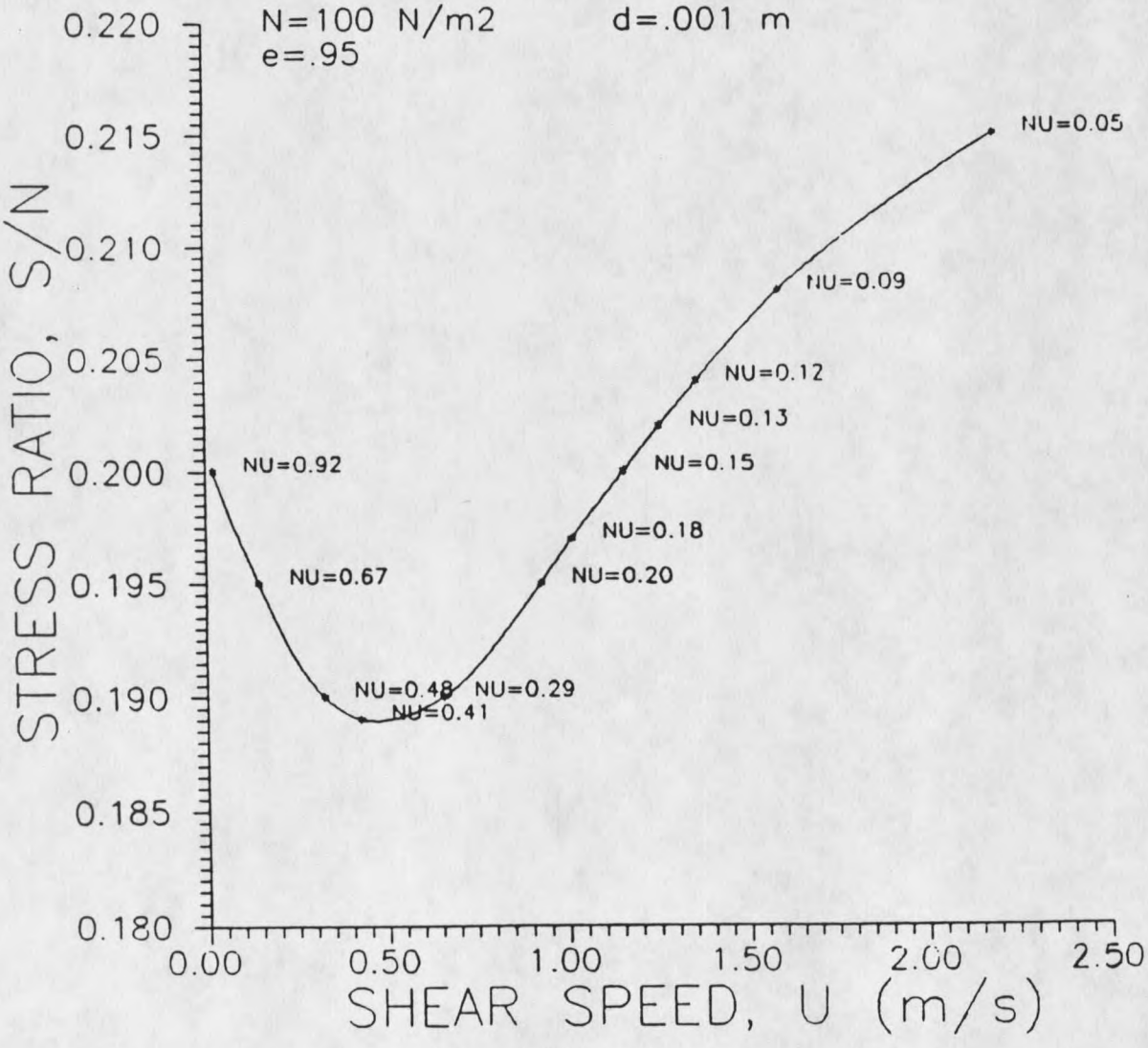

Figure 14

Stress Ratio vs. Shear Velocity from Dent's Numerical Model

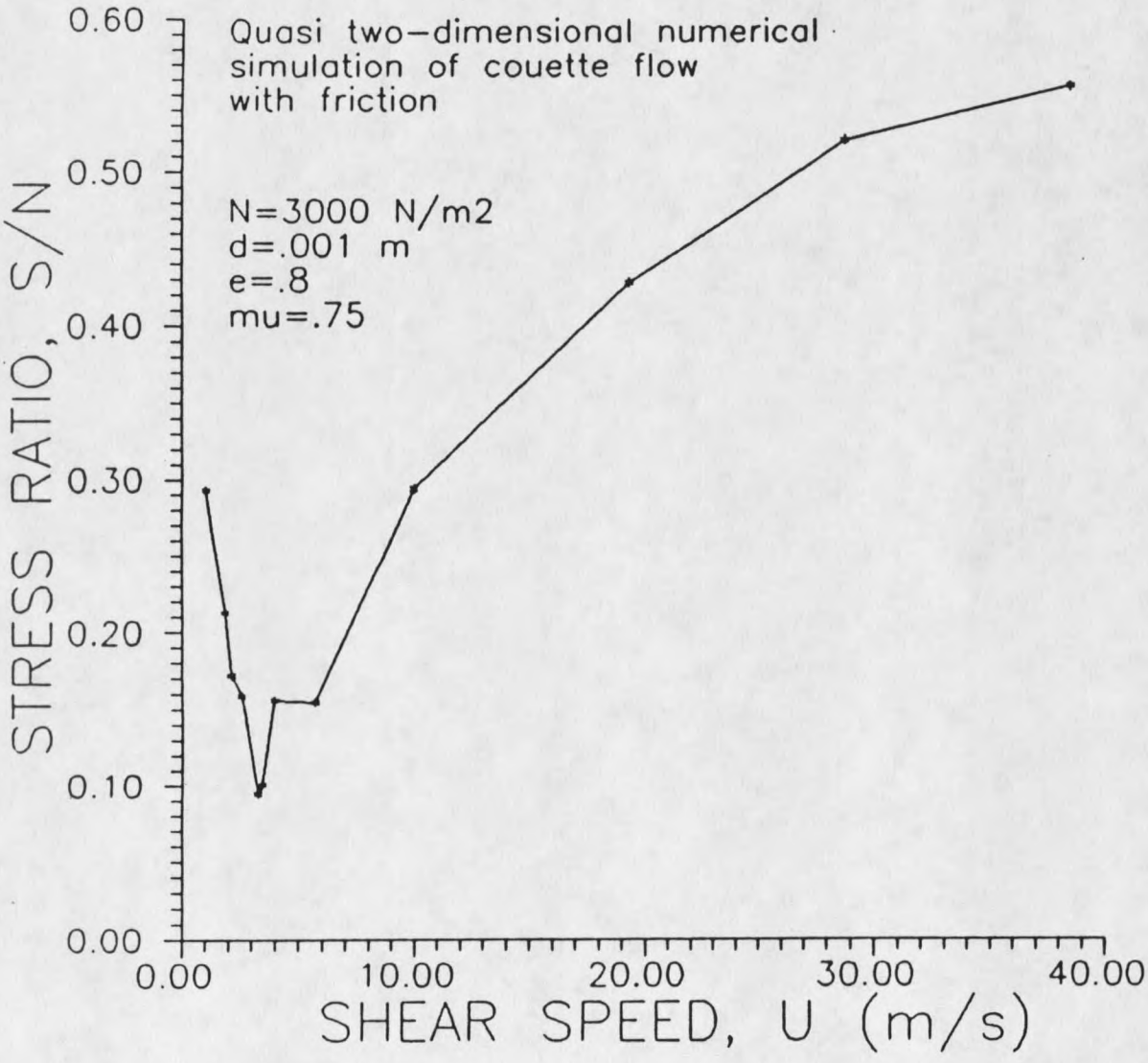

Figure 15

Stress Ratio vs. Shear Velocity from Hanes and Inman
as Reported by Dent

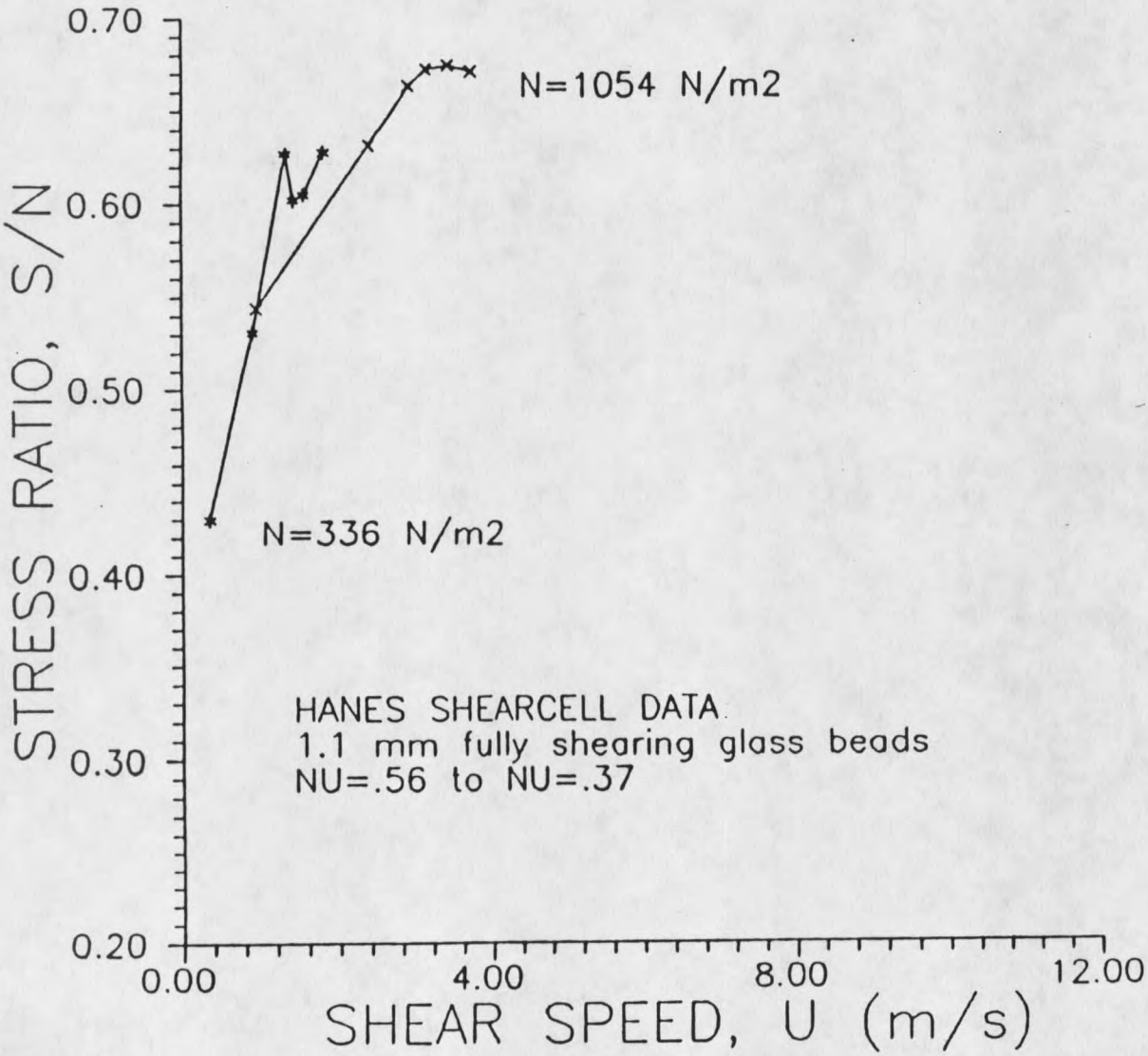

Figure 16

Stress Ratio vs. Shear Velocity from Savage and Sayed
as Reported by Dent

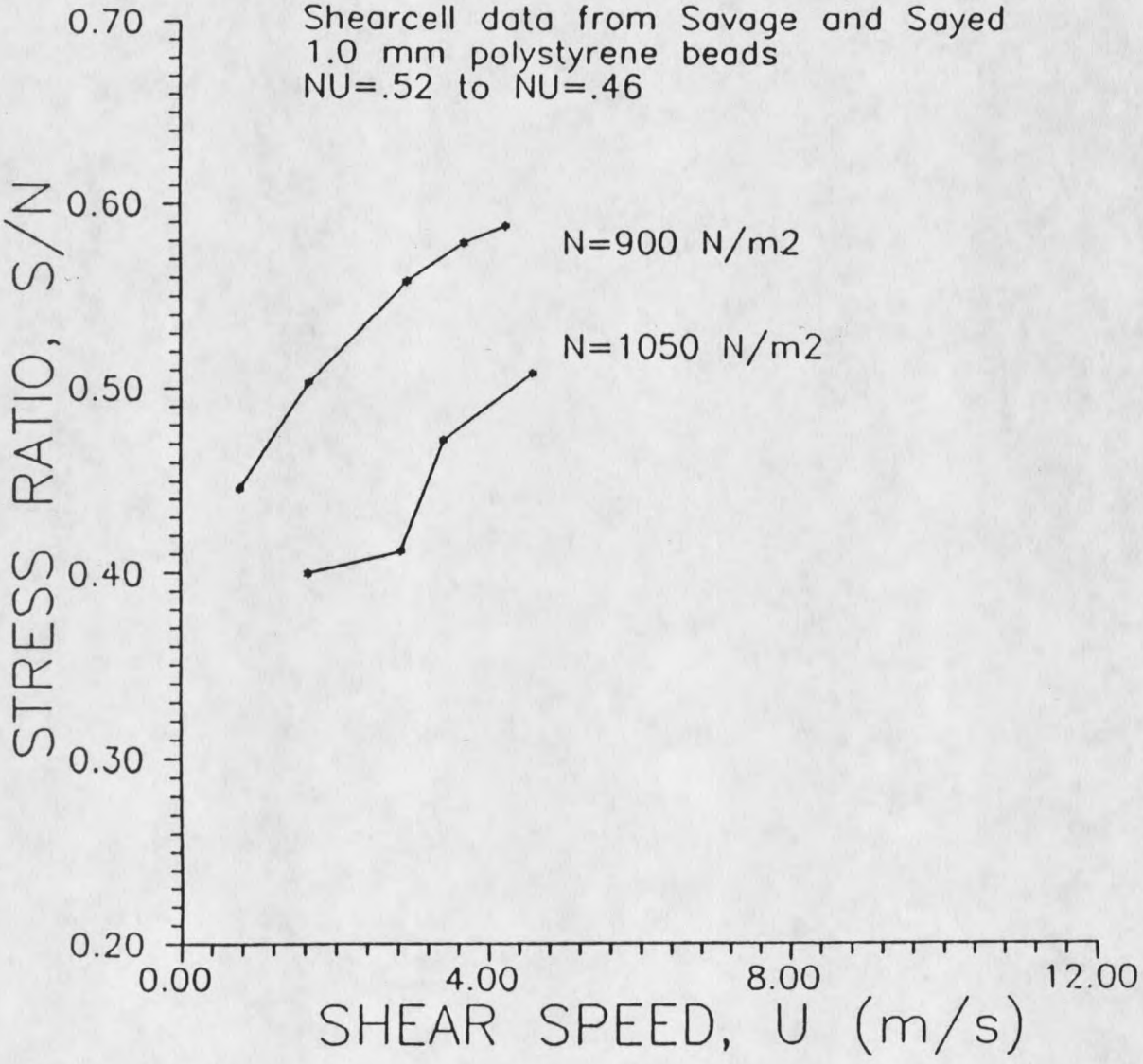

Figure 17

Stress Ratio vs. Shear Velocity from Bridgwater
as Reported by Dent

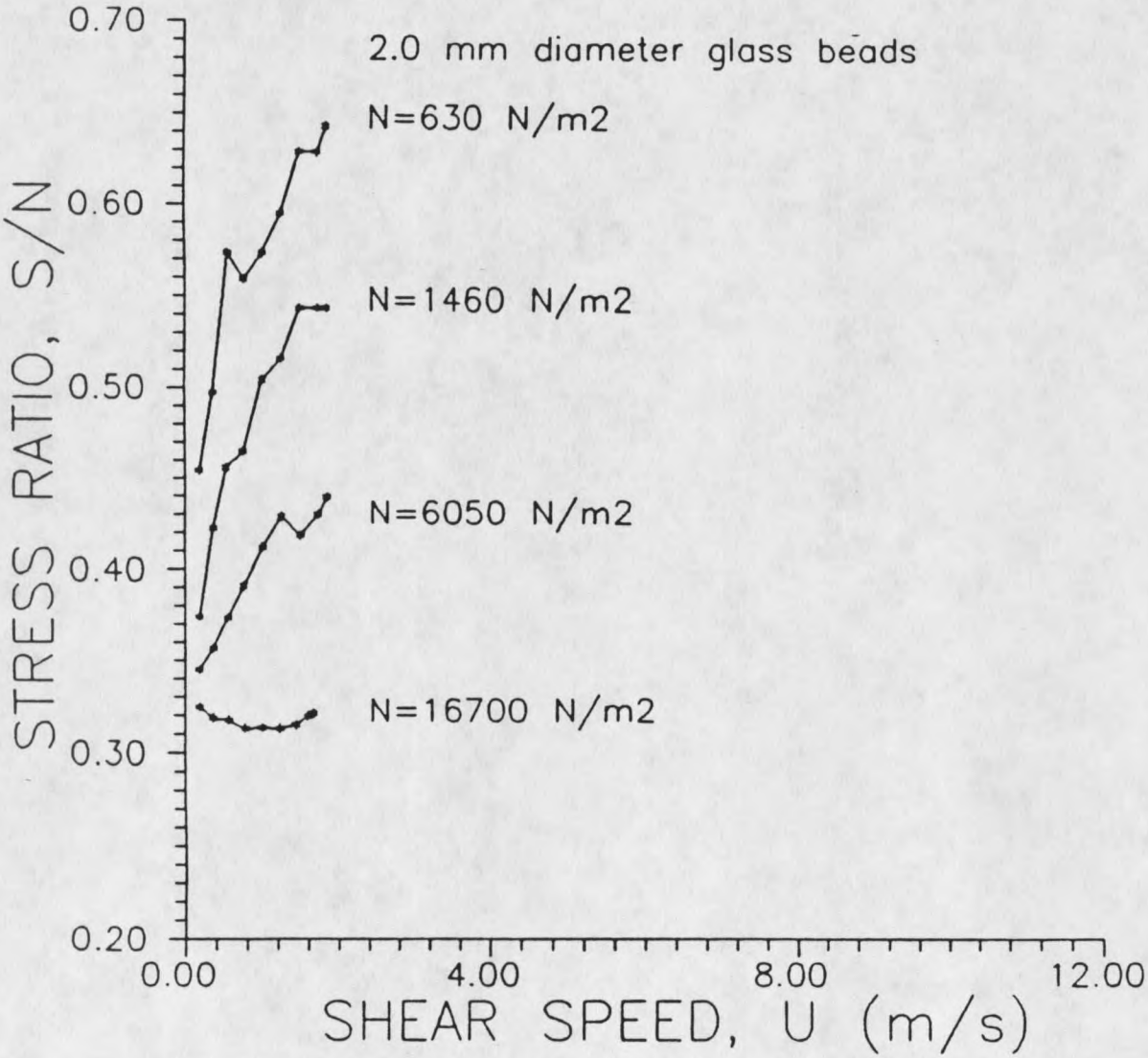

The remainder of this discussion may now be devoted to the results of the numerical model SNOFLO and their implications for the validity of the microstructure hypothesis.

Refer again to Figures 10 through 12. These show the response of the stress ratio to the shear velocity at overburden loads of 2, 15, and 32 kPa. All three show the stress ratio to be quite low initially. The stress ratio then rises with the shear speed until it levels off at a maximum value. This maximum stress ratio is fairly constant for the different overburdens, being about .26 for 2 kPa and about .25 for both the 15 kPa and the 32 kPa normal pressures. The slope of the stress ratio, however, does change with the overburden. As the load on the shearing layer increases, the slope of the stress ratio declines significantly, from attaining the maximum stress ratio at a shear velocity of 2500 d/s at 2 kPa normal pressure to a shear velocity of 8000 d/s at 32 kPa normal pressure. This behavior is verified by the results of Hanes and Inman (Figure 15), Savage and Sayed (Figure 16) and Bridgwater (Figure 17). This indicates that the size effect is due not to a decrease in the maximum stress ratio, but to a decrease in the slope of the stress ratio. Therefore, as a small flow accelerates, its drag will increase quickly with its speed, causing it to stop accelerating at a fairly low velocity. A large event, on the other hand, will not see the drag increase at nearly the same rate, allowing it to attain much higher speeds before reaching equilibrium. It is very likely that this is the principal cause of the size effect. It remains to be seen if the microstructure concept accounts for this decrease in the stress ratio slope. The next series of graphs, Figures 18 through 22, are concerned with changes in the shearing region's behavior as the shear speed is held constant at 5000 d/s while the overburden pressure is increased from 2 to 40 kPa.

Figure 18 shows the relationship of flow depth to overburden. The depth of the fluidized layer drops from 4.05 d (diameters) at a normal pressure of 2 kPa to about 3.55 diameters at 40 kPa normal pressure. This constitutes a compression of 14 percent for the indicated load increase. While in a real flow the effects of scour or gouging may maintain or increase the actual depth of the shearing layer with increasing overburden, the entrainment of new particles into the flow will increase its density (in particles/unit volume). Therefore, while the actual shortening of the shear layer in SNOFLO may be artificial, the increase in particle density which it represents corresponds directly to conditions in real flow. This result, though somewhat trivial, verifies the first prediction of the microstructure hypothesis.

Figure 19 shows the variation of the stress ratio S/N with overburden pressure. Again, the shear speed is constant at 5000 d/s. There is a strong inverse relationship between the normal pressure and the stress ratio. Over the full pressure range, the stress ratio drops from about .26 to about .21. The most significant drop takes place at pressures less than 20 kPa, after which it drops more slowly. This is probably due to a lower rate of bed compression after this point, as indicated in Figure 18. Comparing Figures 18 and 19 there seems to be a strong correspondence between the depth (compression) of the shearing region and its stress ratio. This drop can also be observed in Figures 10, 11, and 12 as a function of the stress ratio slope. This plot, then, shows the size effect manifested at a constant shear speed.

Figures 20 and 21 display information about the number and type of particle collisions occurring within the shearing region as functions of the overburden. Figure 20 is a plot of the contact time fraction versus overburden. The contact time fraction is the

fraction of any given interval of time that sees at least one collision in progress. Figure 21 is a plot of the multiple contact fraction, which is the fraction of those collisions counted in Figure 20 which involve more than two particles. These plots show a strong increase in both binary and multi-particle collisions as the layer is compressed by increasing load. The overall collision rate increases from about 30 percent of the time at the lowest overburden to over 80 percent of the time at the highest, while multiple collisions increase from almost none to about 60 percent of all collisions over the same range. These plots serve to verify the second prediction of the microstructure hypothesis, showing that not only do multi-particle collisions occur, they become the predominate form of particle interaction at high normal pressures.

Figure 22 shows the shear ratio fraction M/S as a function of overburden. M/S is the multiple contact stress ratio M/N divided by the overall stress ratio S/N. The multiple contact stress ratio M/N is simply the ratio of shear stress S to normal stress N exerted on the top block, summed and averaged over only those times that a multi-particle collision is in progress. Thus M/S is a measure of the effect multi-particle microstructures have on the shear strength of the fluidized region. An M/S less than one indicates that microstructures tend to weaken the fluidized layer in shear, while a value greater than one indicates the opposite. Figure 22 shows a good deal of scatter at lower pressures, indicating that the structural shapes and alignment of any microstructures that do form are not uniform, yielding varying effects on the system. Beyond about 10 kPa of normal pressure, M/S stabilizes somewhat between the values of .96 and .99. This means that for the higher overburden pressures microstructures are aligning more uniformly and do yield less shear resistance than do strictly binary collisions. This effect is so small, though, that it may not

even be experimentally significant, and could certainly not cause the almost 20% drop in stress ratio observed in Figure 19. This result tends to discredit the third prediction of this hypothesis, since it shows that microstructures do not seem to present a significantly lower ratio of shear to normal strength than binary collisions do. Data will be presented later to determine if this result is a function of the shear speed or not.

Figure 18

Flow Depth vs. Overburden

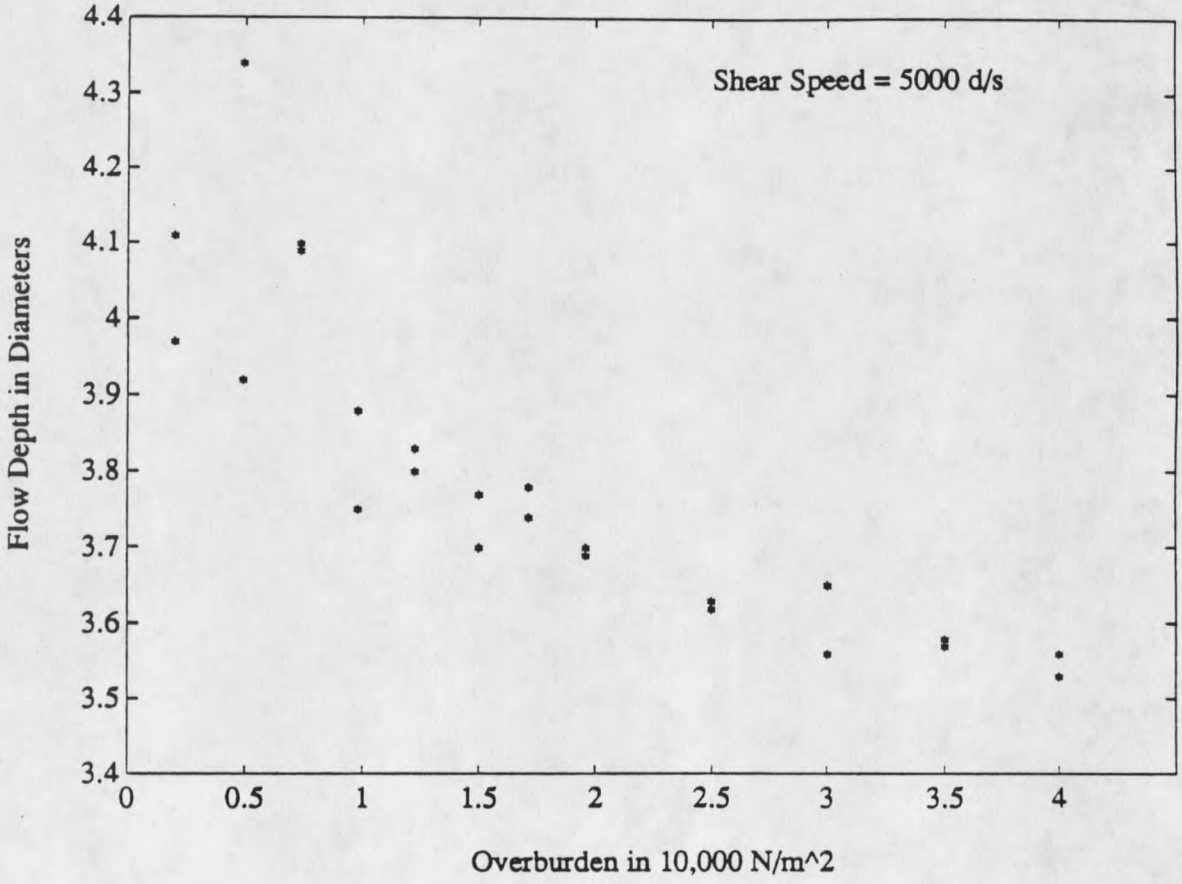

Figure 19

Stress Ratio vs. Overburden

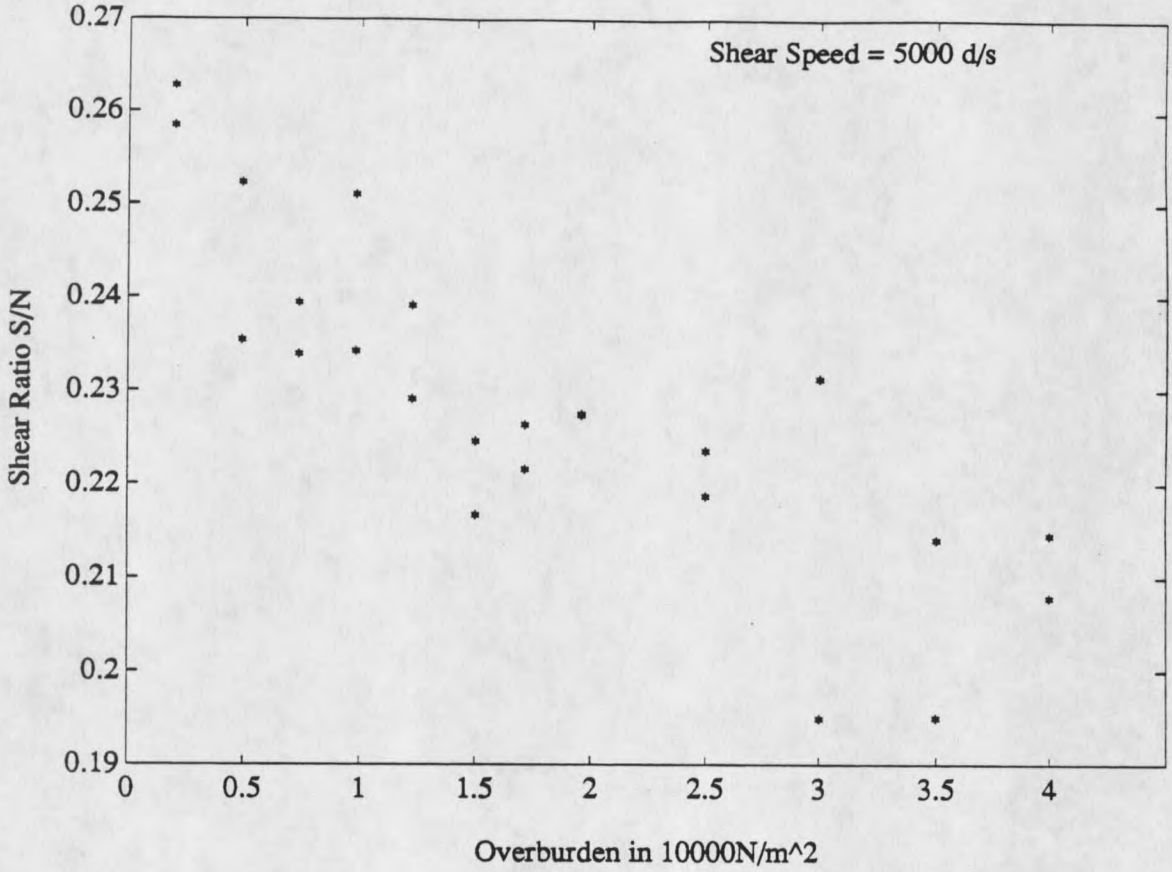

Figure 20

Fraction of Time There are Contacts vs. Overburden

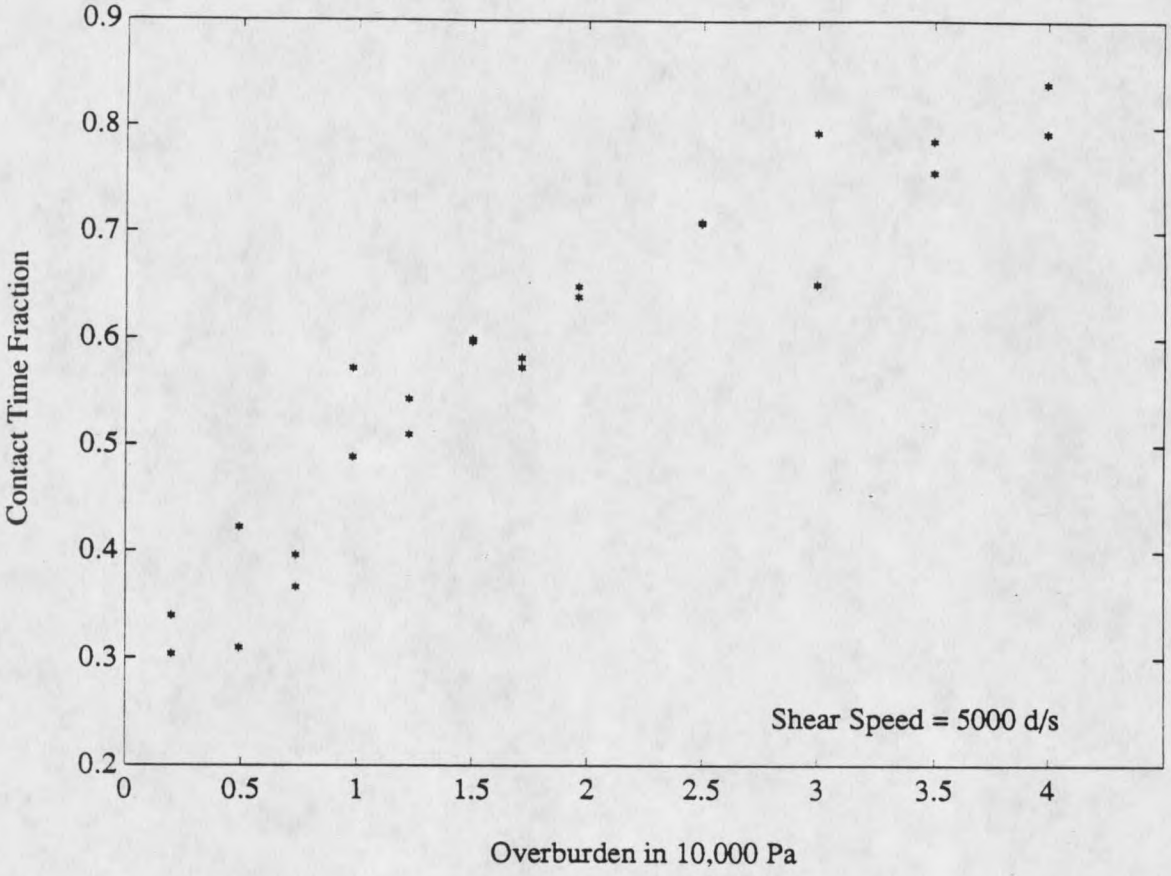

Figure 21

Time Fraction of Contacts that are Multiple vs. Overburden

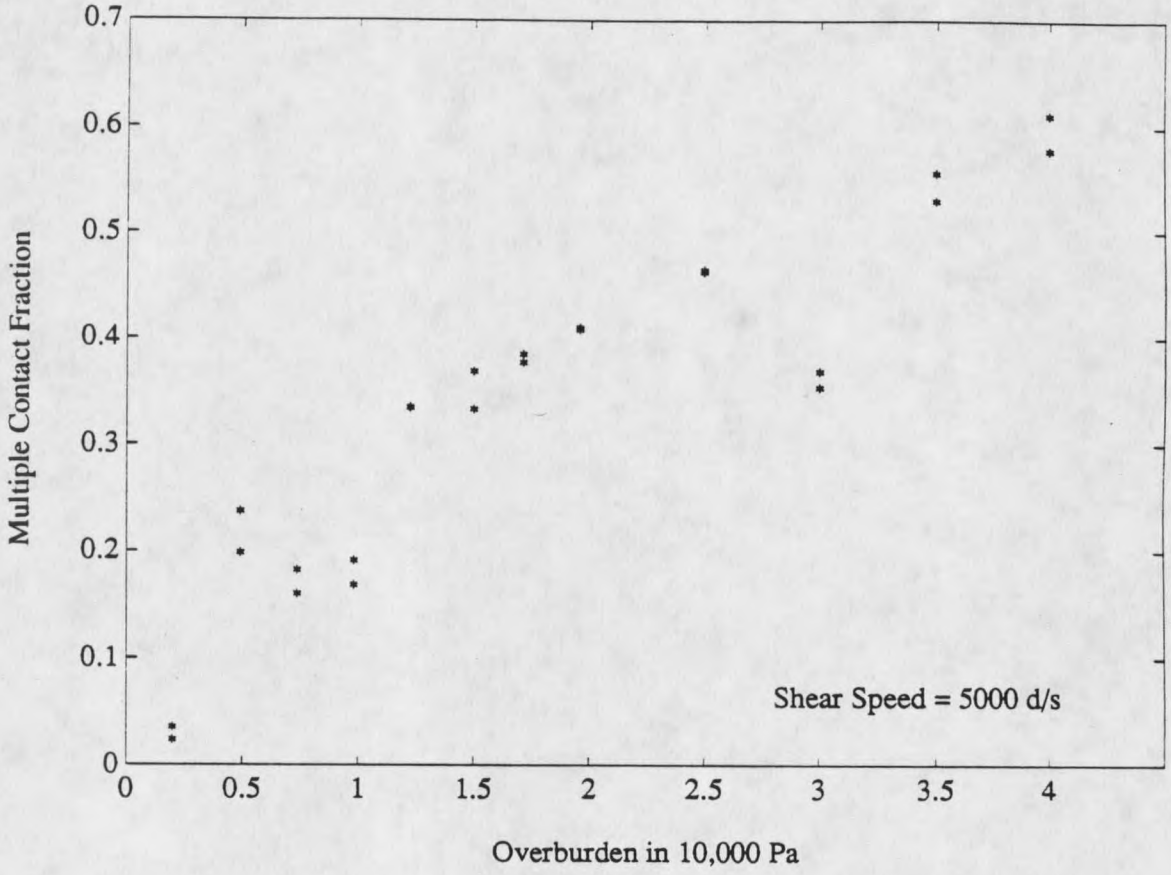

Figure 22

Shear Fraction M/S vs. Overburden

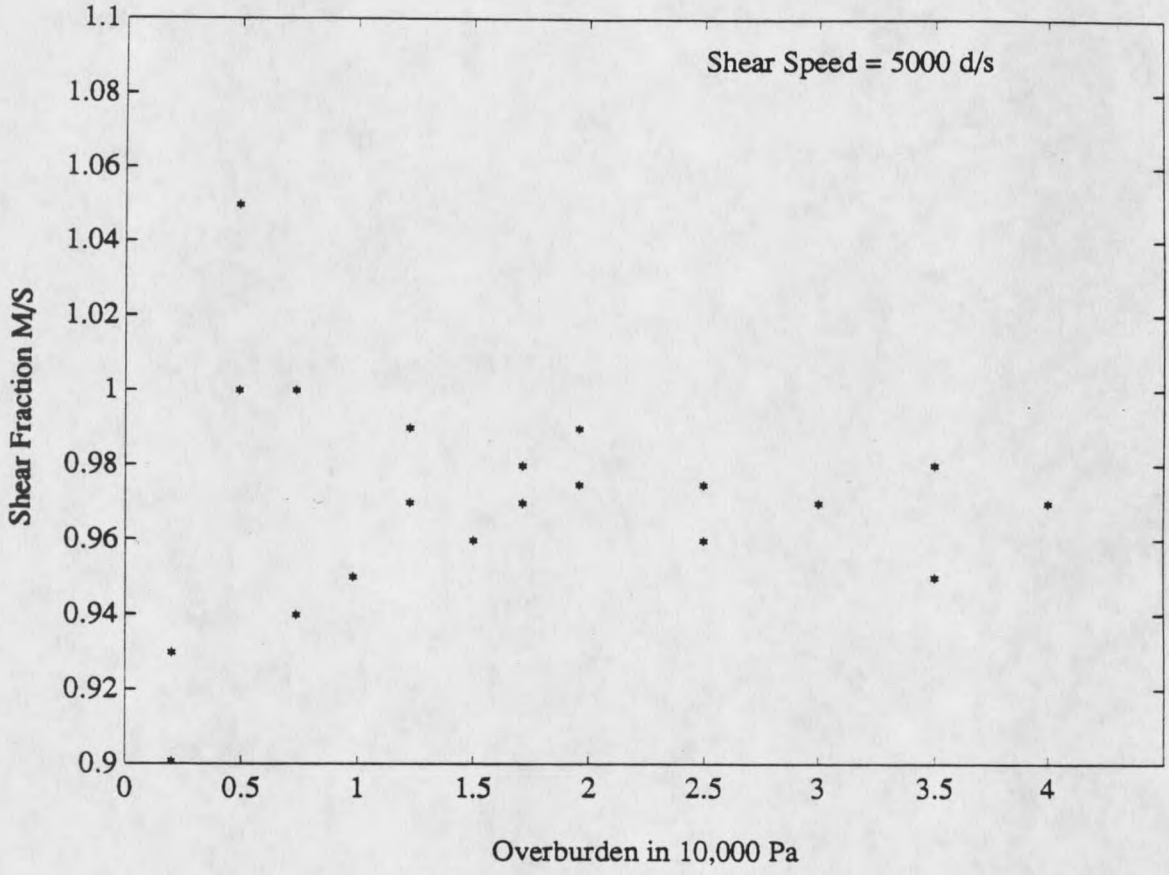

The next series of figures is meant to show additional characteristics of the shearing region for varying shear speeds and constant normal pressures. As in Figures 10 through 12, the shear speed is varied from 500 to 10,000 d/s at three constant overburdens of 2, 15, and 32 kPa. It should be noted here that the highest velocities plotted cannot simply be assumed to have physical meaning, since the strain rate (greater than 2000 /s) may impart so much energy to particle collisions that they survive only due to their non-physical toughness (described earlier). The validity of these high shear strain rates should be checked by physical experiment such as an annular shear cell.

Figures 23, 24, and 25 show the relationship between the depth of the fluidized shearing region and the shear velocity. Each displays similar behavior. The shear region is initially deep at low speeds, and it loses depth as the shear speed increases. At some speed the flow reaches a minimum depth and then begins to dilate again with further increase in shear speed. As normal pressure is increased (from Figure 23 to 25) the shear speed corresponding to the minimum depth increases also. This phenomenon is due to a non-steady-state flow regime occurring at low shear speeds. While this is an artificiality induced by the "shortness" of the flow field in SNOFLO, it may have implications for real granular flows and will be discussed in more detail. In this model, the overburden block may be represented as a mass supported by, but not linked to, an elastic foundation (the dilatant shearing region). As with any spring-mass system, if damping is less than the critical value, any perturbation will cause it to oscillate. In this case, since the mass is not linked to its foundation, this oscillation is not necessarily either sinusoidal or about its equilibrium position. This is a function of the relationship between the stiffness of the foundation and the acceleration of gravity. If the foundation is stiff enough to provide

acceleration greater than that of gravity, then the mass will oscillate about some point above the foundation, and on the average will not be in contact with it. This is analogous to a ball bouncing on the floor.

Figure 23

Flow Depth vs. Shear Velocity at 2 kPa

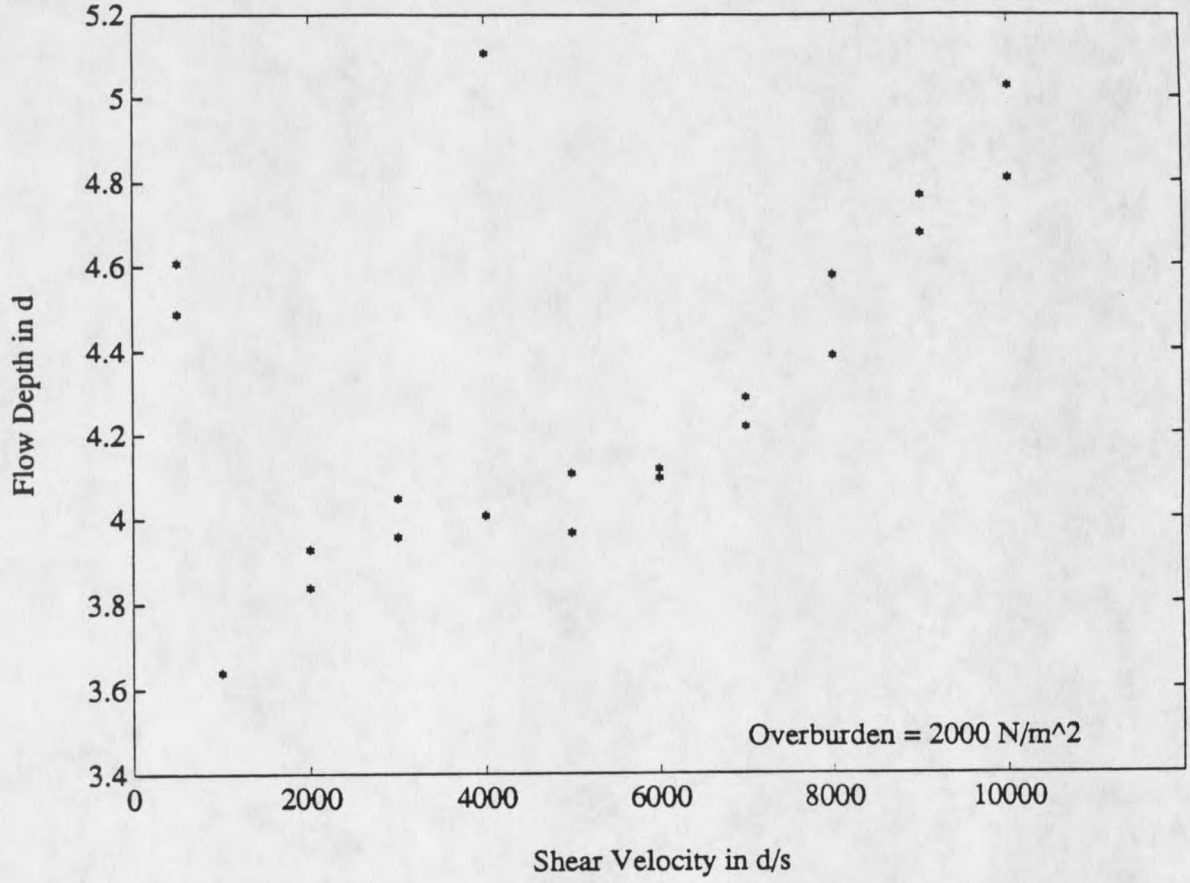

Figure 24

Flow Depth vs. Shear Velocity at 15 kPa

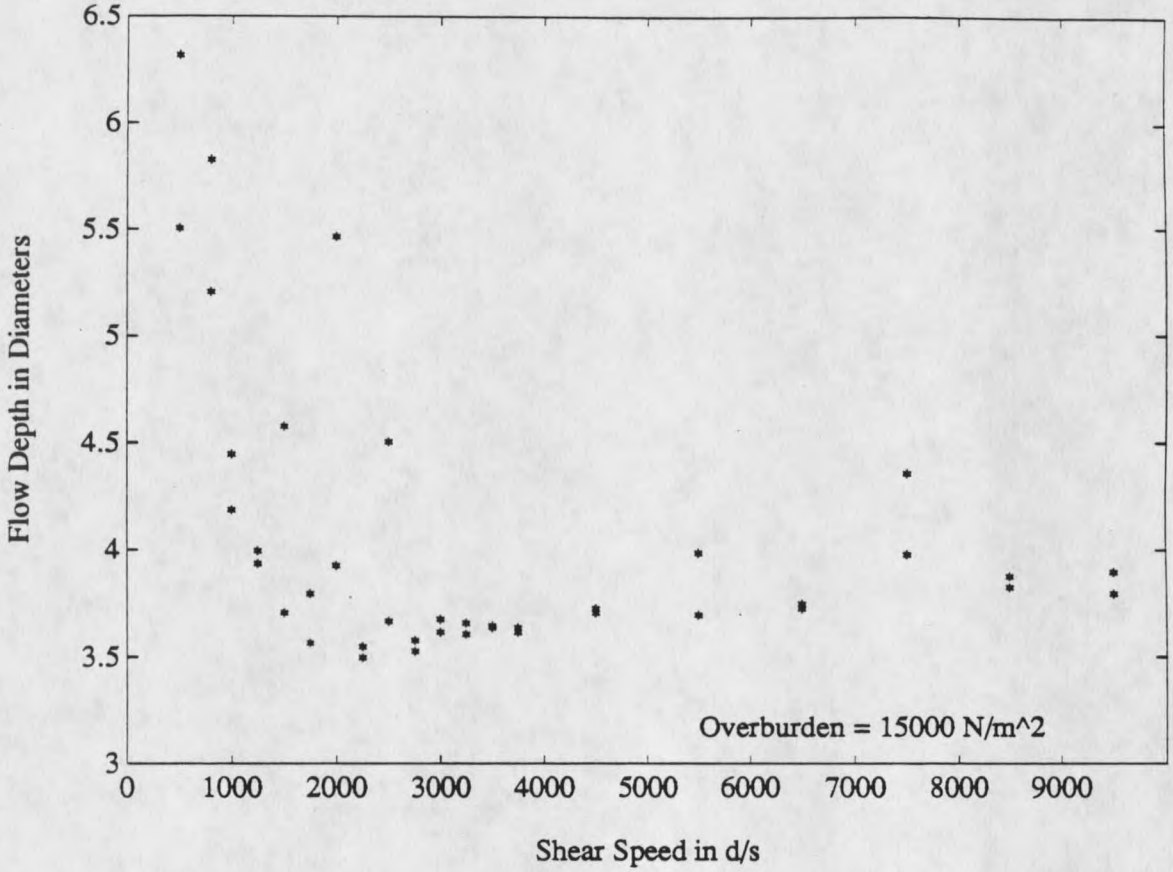

Figure 25

Flow Depth vs. Shear Velocity at 32 kPa

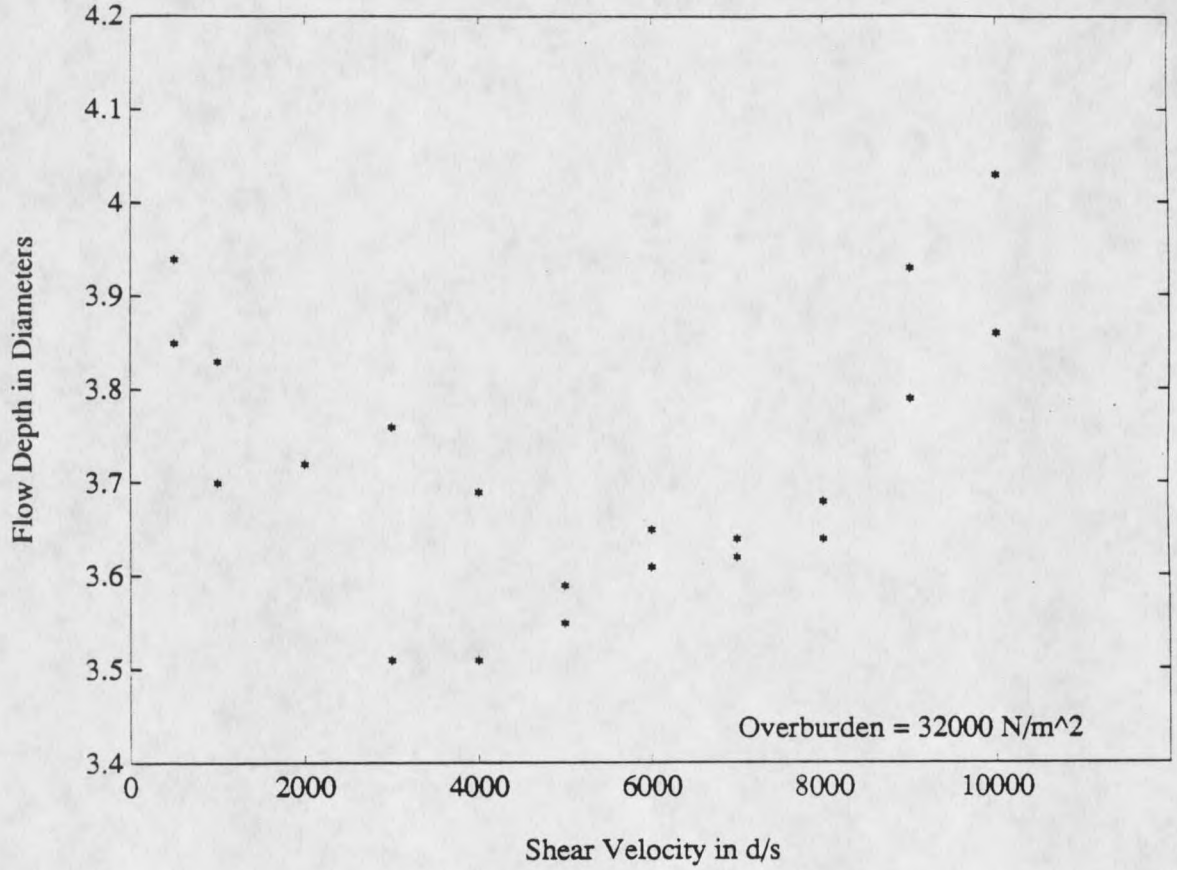

Damping in this system is provided by single particle collisions with the overburden mass. When the mass is above its equilibrium position, gravity is accelerating it downward, converting its potential energy to kinetic energy. Particle collisions with the mass tend to absorb this energy, damping the system. If these particle collisions have enough energy to support the mass so that it settles slowly, then the system is completely damped, and no oscillation will occur. As the overburden mass is increased, more energy is required from these collisions to produce this lift. Since particle energies are a function of the shear speed, higher overburdens require higher shear speeds for steady-state flow. This is apparent from Figures 23 through 25. The minimum flow depth shown in these figures corresponds to the beginning of steady state flow.

After the flow reaches steady-state, the fluidized layer dilates at a fairly even rate with velocity, the rate of expansion being dependent on the overburden. For example, at 2 kPa, the layer dilates from about 3.8 d to about 4.9 d over a velocity range of 9000 d/s, an expansion rate of $12*10^{-5}$ s. At 15 kPa the expansion rate is $7*10^{-5}$ s and at 32 kPa it is about $6*10^{-5}$ s.

The final three figures, 26 through 28, show the shear fraction M/S as a function of shear velocity for the same three overburden pressures. Looking at the three figures, it is apparent that M/S is not a function of velocity. Overburden pressure, though, does have some influence. As overburden is increased, the amount of scatter in the plots decreases significantly, showing that as the shearing region is compressed, microstructures become more consistent in their behavior. However, even for the 32 kPa normal pressure, these microstructures retained 98 to 100 percent of the overall shear strength of the layer. These results, combined with those shown in Figure 22, completely defeat the third prediction of

Figure 26

Shear Fraction M/S vs. Shear Velocity at 2 kPa

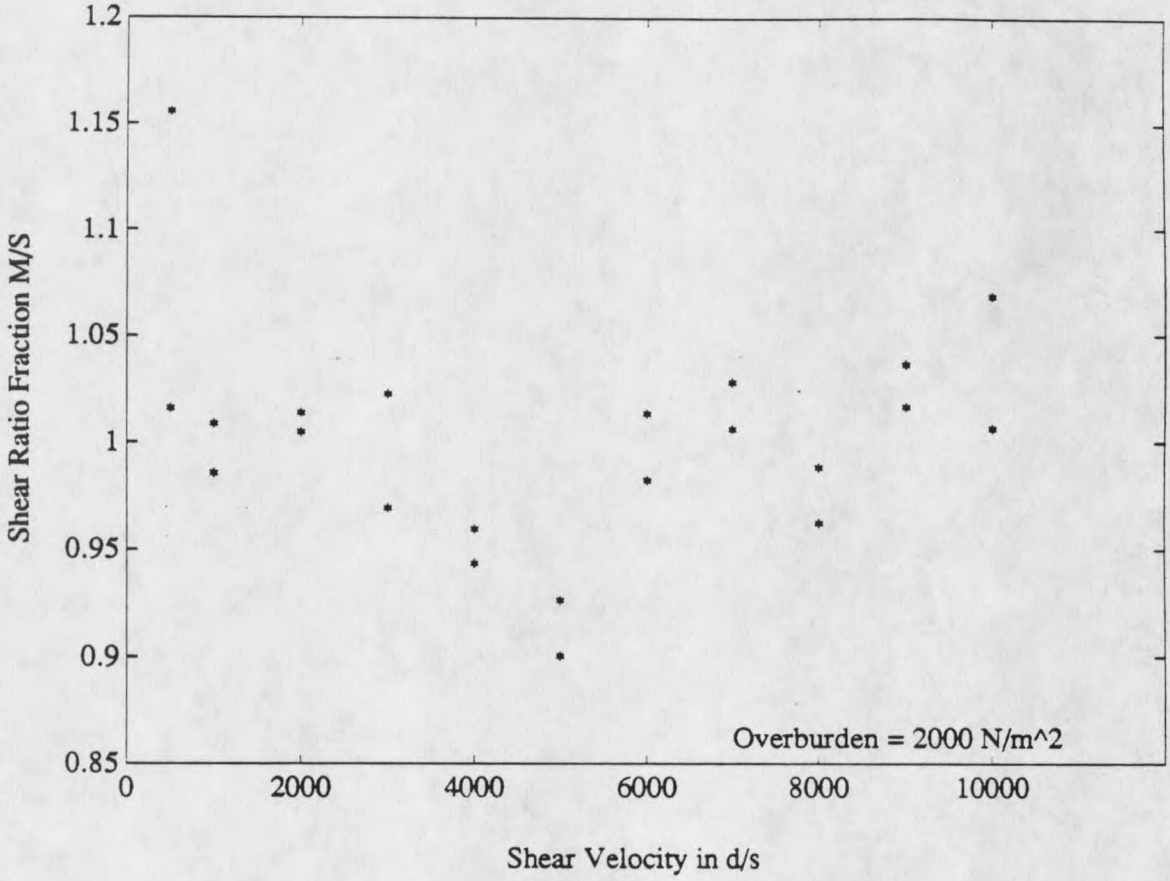

Figure 27

Shear Fraction M/S vs. Shear Velocity at 15 kPa

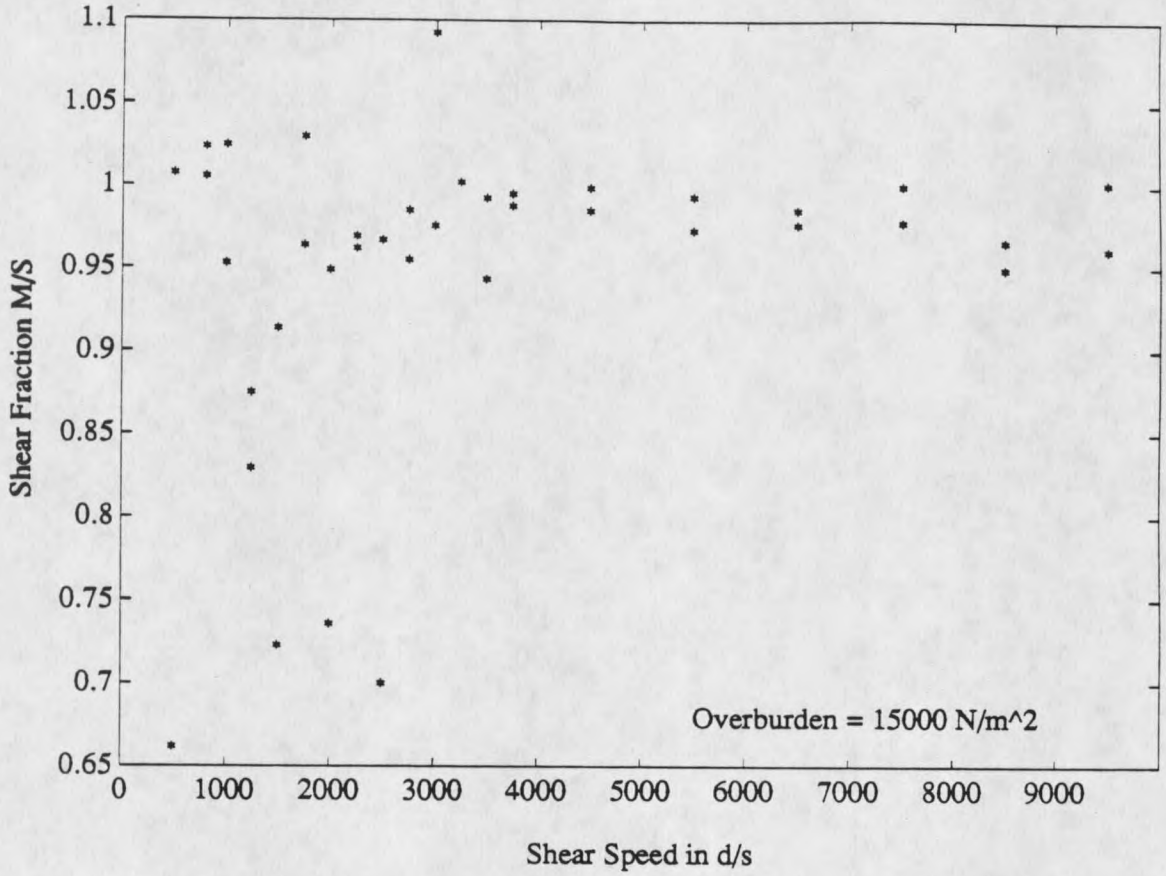

Figure 28

Shear Fraction M/S vs. Shear Velocity at 32 kPa

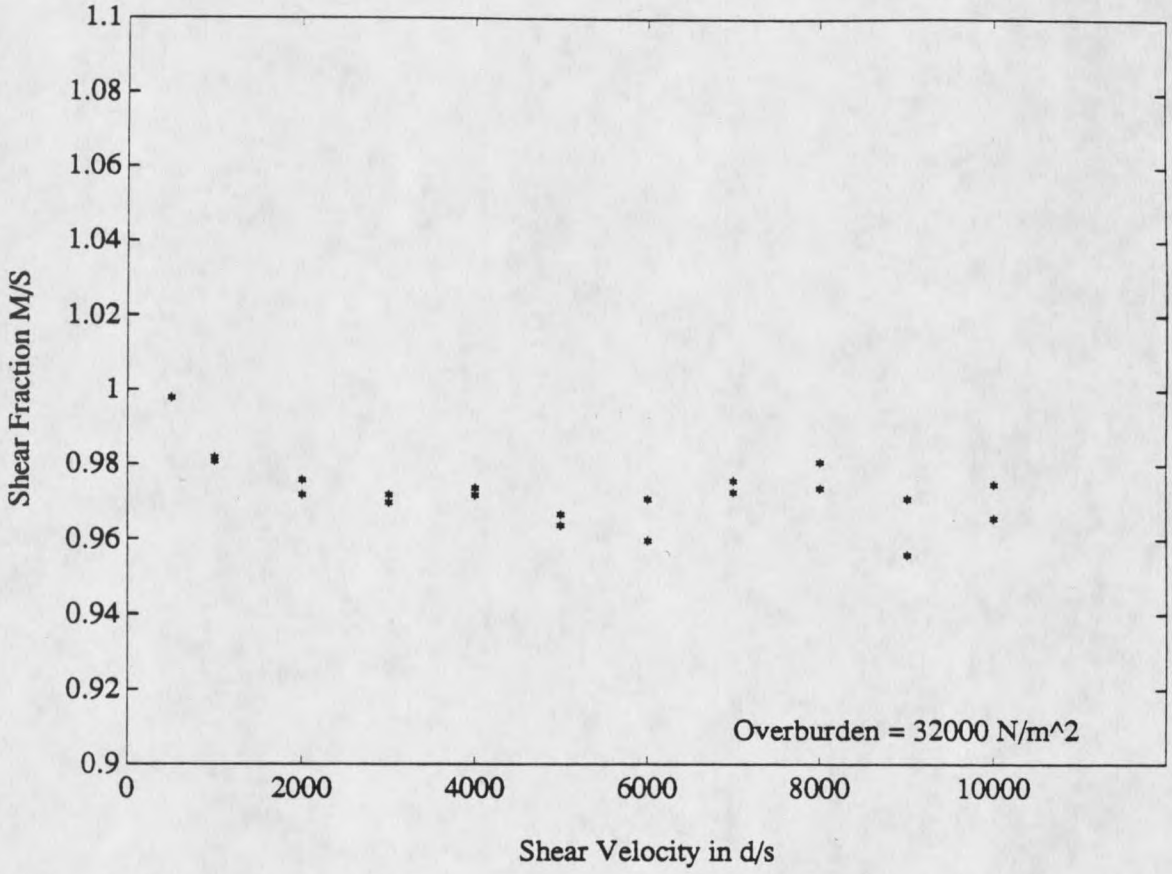

the microstructure hypothesis. Over the entire range of normal pressures, from 2 to 40 kPa, and the entire shear speed range of 500 to 10,000 diameters per second, the microstructures forming in the shearing region failed to show enough difference from binary collisions to account for the size effect observed in this model.

Conclusions

The results just presented lead to the following conclusions.

First, the numerical model SNOFLO yields results consistent with both the theoretical and the experimental results of previous investigators, and it therefore may be assumed to be valid at least as a first approximation of a real granular shear flow.

Second, a size effect was observed. As overburden is increased the slope of the stress ratio is decreased, although the maximum stress ratio appears to remain relatively constant. This effect would cause large flow avalanches and rockfalls to attain higher speeds with no more internal friction than smaller ones.

Third, although microstructures were observed to occur with increasing frequency for higher overburden loads, their effect on the shear strength of the fluidized shearing layer is negligible, and cannot account for the observed size effect. It should be noted that for an actual flow, these microstructures will have even less effect than in this model, since in order for them to form, particles will have to align in three dimensions instead of just two, making them much less frequent. Therefore, the microstructure hypothesis for the size effect is concluded to be invalid.

Suggestions for Further Research

While it resolves the question of the effect multi-particle collisions have on a fluidized granular shear flow, the current work leaves many more puzzling questions unanswered.

The most immediate question concerns the shape of the stress ratio versus shear speed curve. The mechanism which causes it to dip at low speeds and then rise with increasing speed is still unknown. If this mechanism were discovered, it might automatically answer the question of the size effect. That is, what causes the slope of the shear ratio curve to decrease with increasing overburden?

It is likely that the answers to these questions lie in some parameter of the mechanics of the particle collisions which changes with the normal pressure and shear speed. This might be in the average impact angle or possibly in the uniformity (deviation) of the impact angle. There is also a small possibility that there is a connection with the non-steady state flow regime discussed earlier. Although the actual bouncing of the top block in the simulation was a modeling error, the results produced were in excellent agreement with the experimental results of other investigators. This leads to the idea that this oscillation was possibly a numerical manifestation of some process which actually does occur in the highly activated shearing region in physical flows.

To discover answers to these questions, further research is definitely required. One area of investigation which could prove profitable is physical two-dimensional modeling. Since the results of SNOFLO have shown that the phenomena of greatest interest in granular flows do occur in two dimensions, an annular shear cell that allows only two-dimensional flow could yield valuable results. This is especially true because such a device

would eliminate some of the three dimensional modeling errors associated with the circular motion of annular shear cells, such as the secondary circulation currents noticed by Savage and Sayed in 1984.

A large annular shear cell with a trough only wide enough for one spherical bead has been built here at Montana State University, and is currently undergoing set-up and instrumentation procedures. Proposed investigations with this device include further verification of SNOFLO results, and very high speed filming of the flowing material. This film may show macroscopic structures or cells forming which affect the behavior of the flow.

Other areas of investigation include further numerical modeling and further testing with thick flow annular shear cells.

It is important that investigation in this field continues, as snow avalanche and rockfall run out distances and velocities can never be adequately predicted until the mechanism of their transport is completely understood.

REFERENCES

References

Bagnold, R.A. (1954). Experiments on a Gravity-Free Dispersion of Large Solid Spheres in a Newton Fluid Under Shear. Proc. R. Soc. Lond., A225, 49-63.

Campbell, C.S. (1982). Shear Flows of Granular Materials. (Doctoral Dissertation, California Institute of Technology, 1982).

Davies, T.R.H. (1982). Spreading of Rock Avalanche Debris by Mechanical Fluidization. Rock Mechanics, 15, 9-24.

Dent, J.D. and Lang, T.E. (1980). Modeling of Snow Flow. Journal of Glaciology, Vol. 26, No. 94.

Dent, J.D. (1982). A Biviscous Modified Bingham Model of Snow Avalanche Motion (Doctoral Dissertation, Montana State University, June 1982).

Dent, J.D. and Lang, T.E. (1983). A Biviscous Modified Bingham Model of Snow Avalanche Motion. Annals of Glaciology, 4, 42-46.

Dent, J.D. (1986). Flow Properties of Granular Materials with Large Overburden Loads. Acta Mechanica, 64, 111-122.

Dent, J.D (1988). Presented at the Fall Meeting of the American Geophysical Union, December 5-8, 1988, San Francisco, CA.

Erismann, T.H. (1979). Mechanics of Large Landslides. Rock Mechanics, 12. 15-46.

Fahnestock, R.K. (1978). Little Tahoma Peak Rockfalls and Avalanches, Mount Rainier, Washinton USA. In B. Voight (Ed.), Rockslides and Avalanches, Volume 1. New York: Elesevier Scientific Publishing Company.

Fraser, C. (1978). Avalanches and Snow Safety. New York: Charles Scribner's Sons.

Gubler, H. (1987) Measurements and Modeling of Snow Avalanche Speeds. Avalanche Formation, Movement, and Effects, IAHS Publication number 162.

Guest, J.E. (1971). Geology of the Farside Crater Tsiolkovsky. In G. Fielder (Ed.) Geology and Physics of the Moon, 93-103. Amsterdam, Oxford, New York: Elesevier Scientific Publishing Company.

Howard, K.A. (1973, June 8). Avalanche Mode of Motion: Implications from Lunar Examples. Science, 180.

References--continued

Hsu, K.J. (1975) Catastrophic Debris Streams (Sturzstroms) Generated by Rockfalls. Geological Society of America Bulletin, 85.

Hsu, K.J. (1978) Albert Heim: Observations on Landslides and Relevance to Modern Interpretations. In B. Voight (Ed.), Rockslides and Avalanches, Volume 1. New York: Elesevier Scientific Publishing Company.

Hutter, K., Szidarovszky, F., and Yakowitz, S. (1987). Granular Shear Flows as Models for Flow Avalanches. Avalanche Formation, Movement, and Effects, IAHS Publication number 162.

Jenkins, J.T. and Savage, S.B. (1983). A Theory for the Rapid Flow of Identical, Smooth, Nearly Elastic, Spherical Particles. Journal of Fluid Mechanics, 130, 187-202.

Kent, P.E. (1966). The Transport Mechanism in Catastrophic Rock Falls. Journal of Geology, 74.

LaChappelle, E.R. and Lang, T.E. (1980). A Comparison of Observed and Calculated Avalanche Velocities. Journal of Glaciology, Vol. 25, No. 92, 309-314.

Lang, T.E., Dawson, K.L., and Martinelli, M. Jr. (1979). Application of Numerical Transient Fluid Dynamics to Snow Avalanche Flow, Part 1: Development of Computer Program AVALNCH. Journal of Glaciology, vol. 22, No. 86.

Lang, T.E. and Martinelli, M. Jr. (1979). Application of Numerical Transient Fluid Dynamics to Snow Avalanche Flow, Part II Avalanche Modeling and Parameter Error Evaluation. Journal of Glaciology, vol 22, No. 86.

Lang, T.E. and Dent, J.D. (1983). Basal Surface-Layer Properties in Flowing Snow. Annals of Glaciology, 4, 158-162.

McSaveney, M.J. (1978). Sherman Glacier Rock Avalanche, Alaska, USA. In B. Voight (Ed.), Rockslides and Avalanches, Volume 1. New York: Elesevier Scientific Publishing Company.

Mears, A.I. (1980). A Fragment Flow Model of Dry Snow Avalanches. Journal of Glaciology, vol. 26, no. 94.

Norem, H., Kvisteroy, T. and Evensen, B.D. (1985). Measurement of Avalanche Speeds and Forces: Instrumentation and Preliminary Results of the Ryggfonn Project. Annals of Glaciology, 6, 19-22.

References--continued

Norem, H., Irgens, F. and Schieldrop, B. (1987). A Continuum Model for Calculating Snow Avalanche Velocities. Avalanche Formation, Movement, and Effects, IAHS Publication number 162.

Plafker, G. and Ericksen, G.E. (1978). Nevados Huascaran Avalanches, Peru. In B. Voight (Ed.), Rockslides and Avalanches, Vol. 1. New York: Elesevier Scientific Publishing Company.

Richman, M.W. and Chou, C.S. (1986). Boundary Effects on Granular Shear Flows. Submitted to Journal of Applied Mathematics and Physics, November, 1986.

Salm, B. (1966). Contribution to Avalanche Dynamics. Int. Assoc. Sci. Hydrol. Pub. 69, 199-214.

Salm, B., and Gubler, H. (1985). Measurement and Analysis of the Motion of Dense Flow Avalanches. Annals of Glaciology, 6, 26-34.

Savage, S.B., and Jeffrey, D.J. (1981). The Stress Tensor in a Granular Flow at High Shear Rates. Journal of Fluid Mechanics, 110, 255-272.

Savage, S.B. and Sayed, M. (1984). Stresses Developed by Dry, Cohesionless Granular Materials Sheared in an Annular Shear Cell. Journal of Fluid Mechanics, 142, 391-430.

Shimuzu, H., Huzioka, T., Akitaya, E., Narita, H., Nakagawa, M., and Kawada, K. (1980). A Study on High-Speed Avalanches in the Kurobe Canyon, Japan. Journal of Glaciology, Vol. 26, No. 94, 141-151.

Shreve, R.L. (1968). The Blackhawk Landslide. Geol. Soc. Amer. Spec. Paper 108, 47.

Stadler, R. and Buggish, H. (1985). Influence of the Deformation Rate on Shear Stress in Bulk Solids. E.F.C.E. Publishing Service, 49. Chr. Michelson's Institutt, Bergen.

Voellmy, A. (1955). [English Translation] On the Destructive Force of Avalanches. USDA Forest Service. Alta Avalanche Study Center Translation No. 2, 1964.

Yasue, T., Nakanishi, H., Yoshida, A. and Nakano, M. (1987). Applicaiton of some Numerical Simulation Methods for the Surface Layer Avalanche at Maseguchi, Japan. Avalanche Formation, Movement,and Effects, IAHS Publication number 162.

APPENDICES

APPENDIX A

LISTING OF THE CODE SNOFLO

Figure 29

Listing of the Code **SNOFLO**

```
      PROGRAM SNOFLO

C*****************************************************************
C   WRITTEN BY JEFF LACY  JUNE,1988                              *
C                                                                *
C   THIS PROGRAM IS A TWO DIMENSIONAL MODEL OF A MATRIX OF PARTICLES  *
C   SHEARING BETWEEN A STATIONARY BOTTOM LAYER OF PARTICLES AND A     *
C   SOLID UPPER BLOCK OF PARTICLES MOVING AT A FIXED HORIZONTAL VEL-  *
C   OCITY.  THE UPPER BLOCK IS FREE TO CHANGE ALTITUDE.  PARTICLE     *
C   POSITIONS AND VELOCITIES ARE CALCULATED USING SIMPLE LAWS OF      *
C   MOTION AND IMPACT.                                               *
C                                                                    *
C   THE INITIAL MATRIX IS VARIABLE SIZE, WITH VARIABLE WIDTH PERIODIC *
C   BOUNDARIES.  PERIODIC BOUNDARIES SIMPLY ENSURE THAT WHATEVER      *
C   LEAVES ONE SIDE WILL REENTER THE AREA ON THE OTHER SIDE AT THE    *
C   SAME HEIGHT AND VELOCITY.                                        *
C                                                                    *
C   THE OUTPUT DATA FILE CREATED IS NAMED "SNO.DAT".                 *
C   THIS PROGRAM ALSO CREATES A RESTART FILE, SO THAT IF A RUN IS     *
C   INTERUPTED BEFORE THE TIME FRAME THAT IS DESIRED, THE RUN MAY     *
C   SIMPLY BE RESTARTED WHERE IT WAS INTERUPTED, INSTEAD OF STARTING  *
C   OVER AT THE INITIAL CONFIGURATION.                               *
C                                                                    *
C   ONE MAIN FUNCTION OF THIS MODEL IS TO CHECK FOR MULTIPLE CON-     *
C   TACTS BETWEEN PARTICLES, THE CREATION OF MICRO-STUCTURES          *
C   IN THE MATRIX, AND TO DETERMINE THEIR EFFECT ON THE SHEAR RESIS-  *
C   TANCE OF THE MATRIX.  THEREFORE, IT CONTAINS ROUTINES WHICH       *
C   CHECK FOR THE OCCURANCE OF MULTIPLE COLLISIONS, AND TAKE SEPERATE *
C   SHEAR MEASUREMENTS WHEN THEY ARE DETECTED.  RESULTS ARE CLEARLY   *
C   OUTPUT.                                                          *
C                                                                    *
C   PARAMETERS FOR THE RUN ARE INPUT FROM THE PROGRAM "CNTRL.DAT".    *
C   THESE PARAMETERS ARE:                                            *
C       RESTRT: FLAG TO INDICATE IF RESTARTING LAST RUN (1=YES)      *
C       GRAPH:  FLAG TO INDICATE IF CREATING GRAPHICS   (1=YES)      *
C       K1 & K2: APPROACH AND RETREAT SPRING CONSTANTS OF PARTICLES  *
C                (K1=K2*COEFFICIENT OF RESTITUTION)                  *
C       D:  DIAMETER IN mm OF PARTICLES                              *
C       M:  MASS OF PARTICLES                                        *
C       G:  ACCELERATION OF GRAVITY                                  *
C       MTOP:  MASS OF TOP BOUNDARY LAYER                            *
C       NHT:   NUMBER OF ROWS (OF PARTICLES) IN INITIAL MATRIX       *
C       NWID:  NUMBER OF COLUMNS IN INITIAL MATRIX                   *
C       TWID:  WIDTH (IN # OF PARTICLES) OF BOUNDARY LAYERS          *
C       VXT:   HORIZONTAL VELOCITY OF TOP BOUNDARY LAYER             *
C       STEP:  TIME INTERVAL FOR CYCLES WITH CONTACT OCCURING        *
C       LOOP:  AMOUNT OF TIME, IN s, BETWEEN DATA (AND GRAPHICS) O/P *
C       TIME:  DESIRED TIME OF TOTAL RUN                             *
C                                                                    *
C   NOTE:  ANY DIMENSIONALLY CONSISTENT SYSTEM OF UNITS MAY BE USED  *
C   FOR DIMENSIONED VARIABLES IN THIS CODE.                          *
C*****************************************************************

      PARAMETER(N=100)
      INTEGER NHT,NWID,TWID,NUM,I,J,NMTRX,NMOV,NTOT
      INTEGER CONFLG(-N:N),AFLG(-N:N,-N:N),DFLG(-N:N,-N:N)
      INTEGER CYCL,CYCLTOT,GRAPH,MULTI
      REAL D,M,G,VXT,VYT,YT,FXT,FYT,FXB,FYB,T,TCON,TIME,W,MTOP,STEP
      REAL VJMP,VFAC,V,VMAX,TLOOP,TTOT,TFRAC,K1,K2,K,CYCLCON,LOOP,FTOP
      REAL CYCFRAC,TSHEAR,BSHEAR,TSHR,BSHR,DMAX(-N:N,-N:N)
      REAL X(-N:N),Y(-N:N),VX(-N:N),VY(-N:N),AX(-N:N),AY(-N:N)
      REAL XO(-N:N),YO(-N:N),VXO(-N:N),AXO(-N:N),AYO(-N:N),SHRMLT
      REAL VYO(-N:N),S(-N:N,-N:N),SLD(-N:N,-N:N),SLDR(-N:N,-N:N)
      REAL DELTA(-N:N,-N:N),DELNOT(-N:N,-N:N),TTI(-N:N,-N:N)
      REAL VXAV(-N:N),VYAV(-N:N),VXAVG(-N:N),VYAVG(-N:N)
      REAL XAV(-N:N),YAV(-N:N),XA(-N:N),YA(-N:N),MULFRAC
```

Figure 29--continued

```
      REAL AXAV(-N:N),AYAV(-N:N),AXAVG(-N:N),AYAVG(-N:N)
      INTEGER RESTRT,CNFLAG(-N:N,-N:N)

      OPEN(UNIT=10,FILE='CNTRL',STATUS='OLD')
      OPEN(UNIT=11,FILE='SNO',STATUS='NEW')

C*************************************************************************
C     ** READ DATA FROM FILE 'CNTRL.DAT'.  IF 'RESTRT'=1, THEN LAST RUN
C        IS TO BE CONTINUED, AND DATA WILL BE READ FROM FILE 'RESTART.DAT'.
C        OTHERWISE, INCREMENTED VARIABLES ARE SET TO ZERO, AND PARTICLES
C        ARE GIVEN INITIAL POSITIONS & VELOCITIES.
C        IF 'GRAPH' =1, THEN A 'PICTURE' OF THE PARTICLES IS CREATED AT
C        EVERY DATA OUTPUT TIME. **

      READ(10,*) RESTRT,GRAPH
      READ(10,*) K1,K2,D,M,G,MTOP
      READ(10,*) NHT,NWID,TWID,VXT
      READ(10,*) STEP,LOOP,TIME

      IF (RESTRT.EQ.1)THEN
C     **  RESTART OLD RUN **
       OPEN(UNIT=12,FILE='RESTART',STATUS='OLD')
       READ(12,*) NMTRX,NMOV,NTOT
       READ(12,*) VYT,YT,TTOT,CYCLTOT
       DO 10,I=1,NTOT
        READ(12,950)X(I),Y(I),VX(I),VY(I)
10     CONTINUE
       CLOSE(UNIT=12, STATUS='DELETE')
       WRITE(*,*)'             RUN RESTARTED'
       WRITE(11,*)'             RUN RESTARTED'
       GOTO 51
      ELSE

C     **  INITIALIZE NEW RUN **
       CYCLTOT=0
       CYCL=0
       TTOT=0
       NUM=0
       DO 30,I=1,NHT
        DO 20,J=1,NWID
         NUM=NUM+1
         X(NUM)=J*D
         Y(NUM)=I*D
         VX(NUM)=VXT*I/(NHT+1)
         VY(NUM)=(-1)**NUM *.001*VX(NUM)
20      CONTINUE
30     CONTINUE
       NMTRX=NUM

       I=NHT+1
       YT=(I-.05)*D
       DO 40,J=1,TWID
        NUM=NUM+1
        X(NUM)=(J-.5)*D
        Y(NUM)=YT
        VX(NUM)=VXT
40     CONTINUE
       NMOV=NUM

       I=0.E0
       DO 50, J=1,TWID
        NUM=NUM+1
        X(NUM)=(J-.5)*D
        Y(NUM)=I*D
50     CONTINUE
```

Figure 29--continued

```
          NTOT=NUM
          ENDIF
C       ** INITIALIZE MIRROR ELEMENTS **
51          DO 52,I=1,NTOT
             X(-I)=X(I)-TWID*D
             Y(-I)=Y(I)
             VX(-I)=VX(I)
             VY(-I)=VY(I)
52          CONTINUE
C       ** OUTPUT INITIAL CONDITIONS **
            WRITE(*,55)
            WRITE(*,56)NHT,NWID,TWID,NMTRX,NMOV,NTOT
            WRITE(11,55)
            WRITE(11,56)NHT,NWID,TWID,NMTRX,NMOV,NTOT
            WRITE(*,57)
            WRITE(11,57)
            WRITE(*,58) D,M,MTOP,VXT,G,K1,K2
            WRITE(11,58)D,M,MTOP,VXT,G,K1,K2
            WRITE(*,*)'          INITIAL POSITIONS AND VELOCITIES'
            WRITE(11,*)'          INITIAL POSITIONS AND VELOCITIES'
            WRITE(*,930)
            WRITE(11,930)
            DO 54,I=1,NTOT
             WRITE(*,940) I,X(I),Y(I),VX(I),VY(I),AX(I),AY(I),CONFLG(I)
             WRITE(11,940)I,X(I),Y(I),VX(I),VY(I),AX(I),AY(I),CONFLG(I)
54          CONTINUE
55          FORMAT(2X,'NHT',2X,'NWID',2X,'TWID',2X,'NMTRX',2X,'NMOV',2X,'NTOT')
56          FORMAT(2X,I3,2X,I4,2X,I4,2X,I5,2X,I4,2X,I4)
57          FORMAT(2X,'DIAM',2X,'MASS',5X,'MTOP',4X,'SPEED',4X,'GRAV',6X,'K1',
     +      6X,'K2')
58          FORMAT(2X,F5.3,2X,F6.4,2X,F6.3,2X,F7.1,2X,F7.1,2X,E10.3,2X,E10.3)

C       ** INITIALIZE PARTICLE SEPARATIONS **
            DO 70,I=-NMTRX,NMTRX
             IF(I.EQ.0)GOTO 70
             DO 60,J=I+1,NTOT
              IF(J.EQ.0) GOTO 60
              S(I,J)=1.001*D
              SLD(I,J)=1.001*D
              SLDR(I,J)=1.001*D
              DELTA(I,J)=0
              DELNOT(I,J)=0
60           CONTINUE
70          CONTINUE
            ISDUN=0
C ------START OF MAIN LOOP-----------------------------------------------------
100       IF(TTOT.LE.TIME)THEN
C       ** RETURN ACCELERATIONS AND CONTACT FLAGS TO ZERO **
            DO 110,I=-NTOT,NTOT
             IF(I.EQ.0)GOTO 110
             AXO(I)=AX(I)
             AYO(I)=AY(I)
             AX(I)=0
             AY(I)=0
             CONFLG(I)=0
110         CONTINUE
            TO=T
            T=STEP
```

Figure 29--continued

```
C     ** FOR PARTICLES IN BOUNDS, FIND SEPARATIONS **
      W=(TWID+.5)*D
      MULTI=0
      DO 130,I=-NTOT,NMTRX
       IF(I.EQ.0)GOTO 130
       DO 120,J=I+1,NTOT
        IF((J.EQ.0).OR.((J.LT.0).AND.(I.LT.0)))GOTO 120
        AFLG(I,J)=0
        DFLG(I,J)=0
        CNFLAG(I,J)=0
        IF((X(I).GE.-D/2).AND.(X(I).LE.W))THEN
        IF((X(J).GE.-D/2).AND.(X(J).LE.W))THEN
        IF((ABS(I).LE.NMTRX).OR.(ABS(J).LE.NMTRX))THEN
         SLDR(I,J)=SLD(I,J)
         SLD(I,J)=S(I,J)
         S(I,J)=SQRT((X(I)-X(J))**2 +(Y(I)-Y(J))**2)

C       ** DISPLAY MESSAGE IF TIME JUMP CREATED LARGE OVERLAP **
        IF((CON.EQ.0).AND.((S(I,J).LT.0.95*D).AND.(SLD(I,J).GE.D)))THEN
         WRITE(*,*)CYCLTOT,I,J,'   SEPARATION = ',S(I,J)
         WRITE(11,*)CYCLTOT,I,J,'   SEPARATION = ',S(I,J)
        ENDIF


C       ** SET APPROACH, CONTACT, AND MAX DELTA FLAGS, AND DELNOT **
        IF(S(I,J).LE.D)THEN
         IF(S(I,J).LT.SLD(I,J))THEN
          DELNOT(I,J)=0
          AFLG(I,J)=1
         ENDIF
         IF(S(I,J).GE.SLD(I,J))THEN
          AFLG(I,J)=0
          IF(SLDR(I,J).GE.SLD(I,J))THEN
           DELNOT(I,J)=(D-SLD(I,J))*(1-K1/K2)
          ENDIF
         ENDIF
         DELTA(I,J)=D-S(I,J)-DELNOT(I,J)
         IF(DELTA(I,J).GE.0.E0)THEN
          IF((CONFLG(I).NE.0).OR.(CONFLG(J).NE.0))MULTI=1
          CONFLG(I)=J
          CONFLG(J)=I
          CNFLAG(I,J)=1
         ENDIF
         IF(SLD(I,J).GT.D)DMAX(I,J)=0
         IF(DELTA(I,J).GT.DMAX(I,J))THEN
          DMAX(I,J)=DELTA(I,J)
          DFLG(I,J)=1
         ENDIF
        ENDIF
       ENDIF
       ENDIF
       ENDIF
120     CONTINUE
130    CONTINUE

C     ** IF THERE ARE CONTACTS, GOTO ACCEL CALCULATIONS.  IF
C       THERE ARE NO CONTACTS, FIND TIME JUMP AND GOTO POSITION
C       CALCS. **

       CON=0
       DO 140,I=-NMTRX,NMTRX
        IF(I.EQ.0)GOTO 140
        IF(CONFLG(I).NE.0)CON=CON+1
140    CONTINUE
```

Figure 29--continued

```
          IF(CON.EQ.0)THEN
C       **  FIND TIME JUMP TO NEXT COLLISION **
            DO 160,I=-NTOT,NMTRX
             IF(I.EQ.0)GOTO 160
             DO 150,J=I+1,NTOT
              IF((J.EQ.0).OR.((I.LT.0).AND.(J.LT.0)))GOTO 150
              CALL TYMJUMP(X,Y,VX,VY,TTI,I,J,D)
150          CONTINUE
160         CONTINUE
            CALL TIMER(TTI,U,NMTRX,NTOT)
            IF((U.GT.T).AND.(U.NE.1.E-2))T=U
            IF(T+TLOOP.GT.LOOP)T=LOOP-TLOOP
            GOTO 200
          ENDIF

C       ** CALCULATE ACCELERATIONS FOR PARTICLES IN CONTACT **
170       DO 190,I=-NTOT,NMTRX
            IF(I.EQ.0)GOTO 190
            DO 180, J=I+1,NTOT
             IF((J.EQ.0).OR.((I.LT.0).AND.(J.LT.0)))GOTO 180
             IF(CNFLAG(I,J).EQ.1)THEN
              CALL IMPACT(X,Y,DELTA,AFLG,DFLG,AX,AY,I,J,K1,K2,M)
             ENDIF
180         CONTINUE
190       CONTINUE

C       ** FIND NEW PARTICLE POSITIONS AND VELOCITIES **
200       DO 220,I=1,NMTRX
            AX(I)=AX(I)+AX(-I)
            AY(I)=AY(I)+AY(-I)
            X(I)=X(I)+VX(I)*T+.5*AX(I)*T**2
            Y(I)=Y(I)+VY(I)*T+.5*AY(I)*T**2
            VX(I)=VX(I)+AX(I)*T
            VY(I)=VY(I)+AY(I)*T

C        ** IF A PARTICLE MOVES THRU A BOUNDARY LAYER, MOVE IT BACK **
            IF(Y(I).GT.YT)Y(I)=Y(I)-.1*D
            IF(Y(I).LT.0)Y(I)=Y(I)+.1*D
220       CONTINUE

C       ** FIND FORCES ON TOP AND BOTTOM LAYERS **
          DO 230,I=NMTRX+1,NMOV
            AX(I)=AX(I)+AX(-I)
            AY(I)=AY(I)+AY(-I)
            FXT=FXT+AX(I)*M
            FYT=FYT+AY(I)*M
230       CONTINUE
          DO 240,I=NMOV+1,NTOT
            FXB=FXB+AX(I)*M
            FYB=FYB+AY(I)*M
240       CONTINUE

C       ** POSITIONS OF PARTICLES IN TOP LAYER **
          YT=YT+VYT*T+.5*(FYT/MTOP-G)*T**2
          VYT=VYT+(FYT/MTOP-G)*T
          XT=VXT*T
          DO 250,I=NMTRX+1,NMOV
            Y(I)=YT
            VY(I)=VYT
            X(I)=X(I)+XT
250       CONTINUE

C       ** PERIODIC BOUNDARY CONDITIONS **
          BND=TWID*D
          DO 260,I=1,NMOV
            IF(X(I).GT.W) X(I)=X(I)-BND
```

Figure 29--continued

```
          IF(X(I).LT.D/2) X(I)=X(I)+BND

          X(-I)=X(I)-BND
          Y(-I)=Y(I)
          VX(-I)=VX(I)
          VY(-I)=VY(I)
260       CONTINUE

C      ** INCREMENT RUN VALUES **
          TTOT=TTOT+T
          TLOOP=TLOOP+T
          CYCL=CYCL+1
          CYCLTOT=CYCLTOT+1
          IF(CON.NE.0)THEN
           CYCLCON=CYCLCON+1
           TCON=TCON+T
          ENDIF

C      ** TIME SCALED SHEARS EVALUATED, FORCES RETURNED TO ZERO **
          FXTOT=FXTOT+FXT*T
          FYTOT=FYTOT+FYT*T
          IF((MULTI.EQ.1).AND.(FYT.NE.0))THEN
           FXMLT=FXMLT+FXT*T
           FYMLT=FYMLT+FYT*T
           TIMULT=TIMULT+T
          ENDIF
          FXT=0
          FXB=0
          FYT=0

C      ** AVERAGE PARTICLE POSITIONS, VELOCITIES, AND ACCELERATIONS **
          DO 262,I=1,NMOV
           XAV(I)=XAV(I)+X(I)*T
           YAV(I)=YAV(I)+Y(I)*T
           VXAV(I)=VXAV(I)+VX(I)*T
           VYAV(I)=VYAV(I)+VY(I)*T
           AXAV(I)=AXAV(I)+AX(I)*T
           AYAV(I)=AYAV(I)+AY(I)*T
262       CONTINUE

C      ** AT SPECIFIED INTERVAL, WRITE DATA TO FILES **
263       IF(TLOOP.GE.LOOP)THEN
           TFRAC=TCON/TLOOP
           CYCFRAC=CYCLCON/CYCL
           TSHR=0
           SHRMULT=0
           IF(FYTOT.NE.0)TSHR=(FXTOT/FYTOT)
           IF(FYMLT.NE.0)SHRMULT=(FXMLT/FYMLT)
           MULFRAC=TIMULT/TLOOP
           CYCL=0
           TCON=0
           CYCLCON=0
           SHRMLT=0
           TIMULT=0
           FXTOT=0
           FYTOT=0
           FXMLT=0
           FYMLT=0

C      **  AVERAGE POSITIONS, VELOCITIES, AND ACCELERATIONS **
           DO 265,I=1,NMOV
            XA(I)=XAV(I)/TLOOP
            YA(I)=YAV(I)/TLOOP
            VXAVG(I)=VXAV(I)/TLOOP
            VYAVG(I)=VYAV(I)/TLOOP
            AXAVG(I)=AXAV(I)/TLOOP
```

Figure 29--continued

```
            AYAVG(I)=AYAV(I)/TLOOP
            XAV(I)=0
            YAV(I)=0
            VXAV(I)=0
            VYAV(I)=0
            AXAV(I)=0
            AYAV(I)=0
265         CONTINUE
            TLOOP=0

C      **   WRITE TO SCREEN AND DATA FILE **
            WRITE(11,900)
            WRITE(*,900)
            WRITE(11,910)
            WRITE(*,910)
            WRITE(11,920)CYCLTOT,TSHR,SHRMULT,TFRAC,MULFRAC,TTOT,T
            WRITE(*,920) CYCLTOT,TSHR,SHRMULT,TFRAC,MULFRAC,TTOT,T
            WRITE(11,930)
            WRITE(*,930)
            DO 270,I=1,NMOV
             WRITE(11,940) I,XA(I),YA(I),VXAVG(I),VYAVG(I),AXAVG(I),AYAVG(I),
     +       CONFLG(I)
             WRITE(*,945)  I,XA(I),YA(I),VXAVG(I),VYAVG(I),AXAVG(I),AYAVG(I),
     +       CONFLG(I)
270         CONTINUE

C      **   CREATE GRAPHICS **
            IF(GRAPH.EQ.1)THEN
             OPEN(UNIT=14,FILE='PIC',STATUS='NEW')
             DO 275,I=1,NTOT
              WRITE(14,960)X(I),Y(I)
              IF(X(I).GT.(TWID-.5)*D) WRITE(14,960)X(-I),Y(-I)
275          CONTINUE
             CLOSE(UNIT=14)
             CALL PICTURE(NTOT,TWID,D)
            ENDIF

C      **   WRITE TO RESTART FILE **
            OPEN(UNIT=13,FILE='RESTART.DAT',STATUS='NEW')
            WRITE(13,*)NMTRX,NMOV,NTOT
            WRITE(13,*)VYT,YT,TTOT,CYCLTOT
            DO 280, I=1,NTOT
             WRITE(13,950)X(I),Y(I),VX(I),VY(I)
280         CONTINUE
            CLOSE(UNIT=13)
           ENDIF

900        FORMAT('0',2X,'CYCLE',5X,'TOT SHEAR',2X,'MULTI CONTACT',2X,
     +     'PART TIME',2X,'PART TIME',4X,'ELAPSED',5X,'TIME')
910        FORMAT(14X,'RATIO',8X,'RATIO',7X,'W/ CONTACT',2X,
     +     'W/ MULTIS',5X,'TIME',6X,'STEP')
920        FORMAT(1X,I8,2X,E10.3,2X,E10.3,7X,F6.4,5X,F6.4,3X,E10.3,1X,E9.2)
930        FORMAT('0',3X,'I',3X,'AVG X',4X,'AVG Y',4X,'AVG VX',6X,'AVG VY',
     +     6X,'AVG AX',6X,'AVG AY',4X,'CONTACT')
940        FORMAT(1X,I3,2X,F6.3,2X,F6.3,2X,E10.3,2X,E10.3,2X,E10.3,2X,
     +     E10.3,2X,I3)
945        FORMAT(1X,I3,2X,F6.3,2X,F6.3,2X,E10.3,2X,E10.3,2X,E10.3,2X,
     +     E10.3,2X,I3)
950        FORMAT(4X,F6.3,2X,F6.3,2X,E10.3,2X,E10.3)
960        FORMAT(2X,F6.3,2X,F6.3)

           GOTO 100
C----------------------------END OF LOOP-------------------------------
          ELSEIF(ISDUN.EQ.0)THEN
           ISDUN=1
           LOOP=TLOOP
```

Figure 29--continued

```
          GOTO 263
         ENDIF
         CALL DONEPL
         STOP
         END

C     ** END OF MAIN PROGRAM **

C
C*******************************************************************************

           SUBROUTINE TYMJUMP(X,Y,VX,VY,TTI,I,J,D)

C       ** THIS SUBROUTINE FINDS THE TIME TO THE NEXT IMPACT FOR EACH
C          PAIR OF PARTICLES IN THE SYSTEM. **

         PARAMETER(N=100)
         REAL X(-N:N),Y(-N:N),VX(-N:N),VY(-N:N),TTI(-N:N,-N:N)
         REAL C1,C2,C3,C4,RT1,RT2,Q,D
         INTEGER I,J

         C1= (VX(I)-VX(J))**2 + (VY(I)-VY(J))**2
         C2= 2*((X(I)-X(J))*(VX(I)-VX(J)) + (Y(I)-Y(J))*(VY(I)-VY(J)))
         C3= (X(I)-X(J))**2 + (Y(I)-Y(J))**2 - D**2
         C4= C2**2 - 4*C1*C3

         IF((C1.EQ.0).OR.(C4.LT.0))THEN
          TTI(I,J)=1
          GOTO 100
         ELSE
          IF (C2.LT.0.0)THEN
           Q=-0.5*(C2-SQRT(C4))
          ELSE
           Q= -0.5*(C2+ SQRT(C4))
          ENDIF
          RT1=Q/C1
          RT2=C3/(Q+1.E-7)

          IF(RT1.LT.0)RT1=1
          IF(RT2.LT.0)RT2=1
          IF(RT1.LT.RT2)THEN
           TTI(I,J)=RT1
          ELSE
           TTI(I,J)=RT2
          ENDIF
         ENDIF
100      RETURN
         END

C
C*******************************************************************************

         SUBROUTINE TIMER(TTI,U,NMTRX,NTOT)

C     ** THIS SUBROUTINE FINDS THE SMALLEST POSITIVE TIME
C        JUMP TO AN IMPACT. **

         PARAMETER(N=100)
         REAL TTI(-N:N,-N:N),U
         INTEGER I,J,NMTRX,NTOT

         U=1.E-2
         DO 20,I=-NTOT,NMTRX
          IF(I.EQ.0)GOTO 20
          DO 10,J=I+1,NTOT
           IF((J.EQ.0).OR.((I.LT.0).AND.(J.LT.0)))GOTO 10
```

Figure 29--continued

```
          IF(TTI(I,J).LT.U)U=TTI(I,J)
10        CONTINUE
20       CONTINUE
50       RETURN
         END

C
C*******************************************************************************

         SUBROUTINE  IMPACT(X,Y,DELTA,AFLG,DFLG,AX,AY,I,J,K1,K2,M)

C     ** THIS SUBROUTINE CALCULATES ACCELERATIONS BETWEEN CONTACTING
C        PARTICLES. **

         PARAMETER(N=100)
         REAL X(-N:N),Y(-N:N),AX(-N:N),AY(-N:N)
         REAL XA,XB,YA,YB,ACCXA,ACCYA,ACCXB,ACCYB
         REAL ALPHA,DELTA(-N:N,-N:N),K1,K2,K,M
         INTEGER AFLG(-N:N,-N:N),DFLG(-N:N,-N:N),I,J,POSFLG

C     ** SET INTERNAL VARIABLES SO ALPHA SET RIGHT **
              IF(X(I).GE.X(J))THEN
                 POSFLG=1
                 XA=X(J)
                 YA=Y(J)
                 XB=X(I)
                 YB=Y(I)
              ELSE
                 POSFLG=0
                 XA=X(I)
                 YA=Y(I)
                 XB=X(J)
                 YB=Y(J)
              ENDIF
              IF(XB-XA.EQ.0)THEN
               ALPHA=90*(YB-YA)/ABS(YB-YA+.001*D)
              ELSE
               ALPHA=ATAN((YB-YA)/(XB-XA))
              ENDIF
C           ** CHOOSE SPRING CONSTANT **
               IF((AFLG(I,J).EQ.1).AND.(DFLG(I,J).EQ.1))THEN
                K=K1
               ELSE
                K=K2
               ENDIF

C           ** CALCULATE ACCELERATIONS **
              ACCXA= (-K*DELTA(I,J)*COS(ALPHA))/M
              ACCYA= (-K*DELTA(I,J)*SIN(ALPHA))/M
              ACCXB= -ACCXA
              ACCYB= -ACCYA
              IF(POSFLG.EQ.1)THEN
                 AX(I)= AX(I)+ACCXB
                 AY(I)= AY(I)+ACCYB
                 AX(J)= AX(J)+ACCXA
                 AY(J)= AY(J)+ACCYA
              ELSE
                 AX(I)= AX(I)+ ACCXA
                 AY(I)= AY(I)+ ACCYA
                 AX(J)= AX(J)+ ACCXB
                 AY(J)= AY(J)+ ACCYB
              ENDIF
              RETURN
         END

C
```

Figure 29--continued

```
C*******************************************************************************

        SUBROUTINE PICTURE(NTOT,TWID,D)

C    THIS SUBROUTINE CREATES THE PROGRAM GRAPHICS USING DISSPLA LIBRARY.
C    IN ORDER TO RUN, IT MUST BE LINKED (FOR VAX/VMS) BY THE COMMAND
C    "LINK SNOFLO, SYS$DISSPLA:DISSPLALIB/L"
C*******************************************************************************

        PARAMETER(N=100)
        INTEGER I,J,NPIC,NTOT,TWID
        REAL X(N),Y(N),D
        OPEN(UNIT=14,FILE='PIC',STATUS='OLD')
        J=0
        NPIC=NTOT
        DO 10,I=1,NTOT
         READ(14,20)X(I),Y(I)
         IF(X(I).GT.(TWID-.5)*D)READ(14,20)X(-I),Y(-I)
10      CONTINUE
20      FORMAT(2X,F6.3,2X,F6.3)
        CLOSE(UNIT=14,STATUS='DELETE')
        NPIC=NPIC+J
        CALL COMPRS
        CALL AREA2D(6.,10.)
        CALL XNAME('X',1)
        CALL YNAME('Y',1)
        CALL HEADIN('TRY AGAIN$',30,1.0,1)
        CALL GRAF(0.,1.,6.,0.,1.,10.)
        CALL MARKER(16)
        CALL SCLPIC(12.5)
        CALL CURVE(X,Y,NPIC,-1)
        CALL ENDPL(0)
        RETURN
        END

C
C*******************************************************************************
```

APPENDIX B

EXAMPLES OF DATA FROM THE **SNOFLO** SIMULATION

TABLE 1
SHEAR SPEED = 5000 d/s
OVERBURDEN VARYING

OVERBURDEN (Pa)	STRESS RATIO S/N	SHEAR FRACTION M/S	CONTACT TIME FRACTION	MULTI-CONTACT TIME FRACTION	FLOW DEPTH (d)
2000	.2585	.901	.340	.024	3.97
	.2628	.927	.304	.036	4.11
4905	.2355	1.045	.307	.238	4.34
	.2524	1.001	.423	.199	3.92
7357	.2395	1.004	.397	.161	4.09
	.2340	.936	.367	.183	4.10
9810	.2511	.952	.573	.169	3.75
	.2343	.952	.489	.192	3.88
12,262	.2392	.971	.544	.336	3.80
	.2292	.993	.511	.335	3.83
15,000	.2168	.959	.598	.334	3.77
	.2247	.956	.600	.370	3.70
17,167	.2265	.982	.574	.378	3.78
	.2217	.973	.583	.386	3.74
19,620	.2276	.986	.640	.409	3.69
	.2275	.975	.650	.411	3.70
25,000	.2188	.957	.710	.466	3.62
	.2237	.975	.711	.464	3.63
30,000	.1950	.967	.652	.370	3.65
	.2314	.973	.795	.355	3.56
35,000	.2141	.976	.787	.557	3.57
	.1951	.954	.757	.531	3.58
40,000	.2080	.969	.795	.579	3.56
	.2147	.971	.842	.612	3.53

TABLE 2
SHEAR SPEED VARYING
OVERBURDEN = 2 kPa

SHEAR SPEED (d/s)	STRESS RATIO S/N	MULTI-CONTACT RATIO M/N	SHEAR FRACTION M/S	FLOW DEPTH (d)
500	.1535	.1560	1.016	4.49
	.1139	.1316	1.156	4.61
1000	.1661	.1638	0.986	5.23
	.2316	.2336	1.009	3.64
2000	.2402	.2413	1.005	3.93
	.2440	.2474	1.014	3.84
3000	.2589	.2650	1.023	3.96
	.2475	.2401	0.970	4.05
4000	.2636	.2530	0.9598	4.01
	.2312	.2183	0.9442	5.11
5000	.2585	.2329	0.9012	3.97
	.2628	.2437	0.9271	4.11
6000	.2626	.2582	0.9832	4.12
	.2609	.2647	1.014	4.10
7000	.2589	.2661	1.029	4.29
	.2586	.2604	1.007	4.22
8000	.2576	.2548	0.989	4.39
	.2591	.2495	0.963	4.58
9000	.2630	.2675	1.017	4.77
	.2579	.2673	1.037	4.68
10000	.2571	.2747	1.069	4.81
	.2624	.2641	1.007	5.03

TABLE 3
SHEAR SPEED VARYING
OVERBURDEN = 15 kPa

SHEAR SPEED (d/s)	STRESS RATIO S/N	SHEAR FRACTION M/S	FLOW DEPTH (d)
500	.1269	1.008	5.51
	.1236	0.6623	6.32
800	.0798	1.006	5.83
	.0787	1.024	5.21
1000	.0781	1.025	4.45
	.1096	.9535	4.19
1250	.1090	.8756	3.94
	.1705	.8299	4.00
1500	.1724	.7233	4.58
	.1713	.9142	3.71
1750	.1243	.9646	3.80
	.1786	1.0295	3.57
2000	.1474	.7361	5.47
	.1905	.9496	3.93
2250	.2021	.9625	3.55
	.2135	.9697	3.50
2500	.1826	.7004	4.51
	.2060	.9675	3.67
2750	.2142	.9556	3.58
	.2237	.9856	3.53
3000	.2237	.9763	3.62
	.2156	1.0932	3.68
3250	.2203	1.0026	3.66
	.2360	1.0029	3.61
3500	.2365	.9932	3.64
	.2165	.9441	3.65
3750	.2395	.9961	3.64
	.2349	.9886	3.62

TABLE 3-continued

4500	.2278	.9996	3.73
	.2432	.9860	3.71
5500	.2466	.9740	3.70
	.2264	.9943	3.99
6500	.2471	.9973	3.75
	.2444	.9861	3.73
7500	.2475	1.001	3.98
	.2351	.9783	4.36
8500	.2454	.9499	3.88
	.2475	.9665	3.83
9500	.2442	.9615	3.80
	.2480	1.002	3.90

TABLE 4
SHEAR SPEED VARYING
OVERBURDEN = 32 kPa

OVERBURDEN (Pa)	STRESS RATIO S/N	MULTI-CONTACT RATIO M/N	SHEAR FRACTION M/S	FLOW DEPTH (d)
500	.0461	.0401	.870	3.85
	.0408	.0407	.998	3.94
1000	.0664	.0652	.982	3.70
	.0626	.0614	.981	3.83
2000	.1066	.1040	.976	3.72
	.1000	.0972	.972	3.72
3000	.1386	.1347	.972	3.76
	.1821	.1766	.970	3.51
4000	.1642	.1600	.974	3.69
	.2085	.2026	.972	3.51
5000	.2213	.2140	.967	3.55
	.2086	.2010	.964	3.59
6000	.2130	.2069	.971	3.65
	.2202	.2115	.960	3.61
7000	.2369	.2313	.976	3.62
	.2371	.2307	.973	3.64
8000	.2350	.2289	.974	3.68
	.2436	.2389	.981	3.64
9000	.2181	.2086	.956	3.93
	.2234	.2170	.971	3.79
10000	.2162	.2088	.966	4.03
	.2277	.2220	.975	3.86